





# Radiometric Partial Discharge Detection: A Review

Sinda Kaziz <sup>1,2,\*</sup> , Mohamed Hadj Said <sup>3</sup>, Antonino Imburgia <sup>2</sup> , Bilel Maamer <sup>1,3</sup>, Denis Flandre <sup>4</sup>, Pietro Romano <sup>2</sup>  and Fares Tounsi <sup>4,\*</sup> 

<sup>1</sup> Faculté des Sciences de Monastir, Université de Monastir, Monastir 5019, Tunisia

<sup>2</sup> L.E.P.R.E. H.V. Laboratory, Department of Engineering, University of Palermo, 90128 Palermo, Italy

<sup>3</sup> Centre de Recherche en Microélectronique et Nanotechnologie (CRMN), Sousse 4050, Tunisia

<sup>4</sup> SMALL Group, ICTEAM Institute, UCLouvain, 1348 Louvain-la-Neuve, Belgium

\* Correspondence: [sinda.kaziz@fsm.u-monastir.tn](mailto:sinda.kaziz@fsm.u-monastir.tn) (S.K.); [fares.tounsi@uclouvain.be](mailto:fares.tounsi@uclouvain.be) (F.T.)

**Abstract:** One of the most common failures or breakdowns that can occur in high-voltage (HV) equipment is due to partial discharges (PDs). This occurs as a result of inadequate insulation, aging, harsh environmental effects, or manufacturing flaws. PD detection and recognition methods have gained growing attention and have seen great progress in the past decades. Radiometric methods are one of the most investigated detection approaches due to their immunity to electromagnetic interference (EMI) and their capabilities to detect and locate PD activities in different applications such as transformers, cables, etc. Several review articles have been published to classify and categorize these works. Nonetheless, some concepts are missing, and some improvement techniques, such as PD detection at high-frequency (HF) and very high-frequency (VHF), have been overlooked. We present in this paper an exhaustive review study of state-of-the-art PD detection based on radiometric methods at different usable radiofrequency bands (i.e., HF, VHF, and UHF). Accordingly, we propose a new generic categorization approach based on the detected electromagnetic wave component (magnetic or electric fields) and pick-up location, either from free space or ground cable.

**Keywords:** partial discharge detection; HV equipment diagnosis; radiometric detection; inductive sensors; UHF antennas; loop antennas; printed antennas



**Citation:** Kaziz, S.; Said, M.H.; Imburgia, A.; Maamer, B.; Flandre, D.; Romano, P.; Tounsi, F. Radiometric Partial Discharge Detection: A Review. *Energies* **2023**, *16*, 1978. <https://doi.org/10.3390/en16041978>

Academic Editor: Pawel Rozga

Received: 25 December 2022

Revised: 3 February 2023

Accepted: 13 February 2023

Published: 16 February 2023



**Copyright:** © 2023 by the authors. Licensee MDPI, Basel, Switzerland. This article is an open access article distributed under the terms and conditions of the Creative Commons Attribution (CC BY) license (<https://creativecommons.org/licenses/by/4.0/>).

## 1. Introduction

The stability of the electrical insulation in high-voltage (HV) equipment can have a major impact on the lifespan of the apparatus, depending on working conditions and operating stability. In the contemporary electric power industry, technicians and engineers oversee the operation as well as the maintenance of electrical equipment, cables, and machinery that connect electrical substations to power plants [1]. Extending the usable life of electrical apparatus by reducing the potential sources of failure or degradation is a critical part of these experts' tasks [2]. However, a high percentage of failures occur in the insulation system due to the uncontrolled existence of several aging mechanisms of electrical, chemical, thermal, radiation [3], and environmental origin [4]. These phenomena, over time, tend to accelerate the deterioration of the material's dielectric properties, leading to equipment breakdown. One of the important indicators when diagnosing the insulation condition of an electrical asset is the measurement of partial discharge (PD) activity, since its presence can be considered both a cause and a result of most electrical problems in insulation systems [5].

PD activity is a detectable fault that tends to occur in those parts of the insulation of any electrical device where the dielectric strength is low or where there is greater electric field stress [6]. In this respect, it is essential not to exceed the rated operating values to avoid overloading, which could lead to damaging some point or area of the insulation material. However, it has been demonstrated that PD activity can be detected even during operation at nominal voltage levels without causing immediate equipment failure, and its recurrence can lead to progressive insulation deterioration due to electron and ion

attacks and chemical degradation [2,5,7]. PDs can be categorized into four classes based on their nature and location, namely: internal, surface, treeing, and corona [8]. The effect of some PD types can be simulated using the finite element method to examine their adverse effect on the electric field distribution in the insulator [9]. Some types of PD may be less detrimental to material deterioration than others and, once discovered, can be effectively controlled during periodic maintenance work [10,11]. Therefore, the quantification of PD activity in the equipment during the maintenance process is essential, as it will help to accurately assess the severity of possible failures or the appearance of new defects that likely will affect performance in the short, medium, or long term [12]. To obtain sufficient monitoring capabilities for PD detection, various methods have been devised and used for insulation testing, including the conventional electrical method based on IEC 60270 as well as other unconventional approaches [13]. The standard electrical approach is the most widely used due to its efficiency; nevertheless, the existence of disturbances due to external electrical noise and interference during PD testing is a drawback. This noise causes a loss of sensitivity, especially when low-energy PD pulses are present in the HV system. Another disadvantage of PD electrical measurements is the presence of more than one source of the pulse-shaped signal in the HV electric system under examination. In this case, proper selection of the unconventional measurement approach followed by efficient signal processing is required to accomplish an accurate assessment of the insulation condition. Unconventional approaches rely on physical phenomena associated with PD events such as acoustic pressure waves, optical emission [14], chemical byproducts [15], and electromagnetic (EM) waves [16]. Various review articles based on unconventional techniques have been published with different categorization approaches, such as detection methods, localization, and/or domains of application. Ilkhechi and Samimi [17] reviewed the main features and structures of acoustic sensors for PD localization and compared them with the standard electrical method. Various acoustic and combined acoustic-electrical methods in transformers were discussed. Duval [15] wrote a review on PD detection in transformers by the chemical method based on a dissolved gas analysis (DGA). Morsalin and Das [18] presented an overview of various diagnostic aspects of PD measurements and discharge sources (e.g., void, surface, and corona) and their behaviors under varying test voltage frequencies. Over the last few decades, researchers have been lured toward the radiometric PD measurement approach because of its immunity to external electromagnetic interference (EMI) and suitability for on-site testing compared to conventional methods. The rise time of a pulse discharge can be less than one nanosecond, depending on the resonant structure of the insulation defect [19]. Such a short impulse can generate EM waves with frequency components in the ultra-high frequency (UHF) range, i.e., from 300 MHz to 3 GHz [20]. Once the wave hits the ground shield or case/shield ground, it turns into a high-frequency current pulse in the range of 500 kHz to 50 MHz, which is usually centered near 10 MHz, and may travel for dozens of meters along the ground path. Hence, radio-frequency (RF) sensors based on EM wave detection could be divided into three categories: inductive sensors, loop antennas, and VHF/UHF antennas, depending on the detected EM wave component (B- or E-field) and pick-up location, either from free space or ground cable.

Several review articles about PD detection based on RF measurement have been published in recent years, focusing on UHF detection methods [21–25], pattern recognition [12], and localization [26,27]. However, these review articles only focus on listing the different types of UHF sensors used in PD detection in different HV equipment, such as transformers, gas-insulated switchgear (GIS), and cables, without any classification. To advance the current state-of-the-art, we propose in this paper an exhaustive review of PD radiometric sensors, in which we present most concepts and designs operating in useful RF bands (i.e., high frequencies (HF) ranging from 3 to 30 MHz, very high frequencies (VHF) ranging from 30 to 300 MHz, and UHF). All of the radiometric sensors included in this paper rely on detecting the consequences of the EM wave emitted by the flashover of part of the insulation system due to PD activities. The remainder of this paper is organized as

follows: Section 2 describes related background information on how PD is represented and measured and presents the available detection methods. Next, RF sensors for electromagnetic PD detection in different frequency bands (i.e., HF, VHF, and UHF) are presented in Section 3.

## 2. Partial Discharges Overview

### 2.1. PD Background and Types

A PD is a localized dielectric breakdown (that does not completely bridge the gap between the two conductors), caused by a localized electric field greater than the system's dielectric withstand capability, of a small part of an electrical insulation system (solid, fluid, or gas). From the 1990s to the present day, much research has been carried out to investigate PDs, and intriguing publications have been published that detail the physical characteristics of the phenomenon [10,28,29]. PDs exhibit stochastic behavior over time due to the stochasticity of the delay caused by the random availability of the discharge's starting electron and memory impacts caused by prior discharges influencing subsequent ones. Particularly once stimulated, PDs affect the characteristics of the dielectric material and leave behind residual charges trapped on the dielectric surface, which then impact the occurrence of future PDs [30,31]. However, as is well known, an insulation diagnosis is difficult to obtain because characteristics such as the magnitude and timing of the onset of the PD change stochastically.

Partial discharges may be categorized into four types: internal, treeing, surface, and corona discharges, as shown in Figure 1. Internal partial discharges are the most common and are one of the leading causes of premature insulator failure in the electrical power grid. In fact, during the manufacturing process, micro air cavities may get trapped in the dielectric material, and thus, when the insulation is subjected to a high voltage stress, an unbalanced distribution is formed between the electric field present in the air microcavities and that in the surrounding dielectric layer (Figure 1a). Internal PD is a silent defect without sound, smell, or visual indication of a problem prior to failure, which makes it the most harmful. Therefore, the presence of air voids within the dielectric bulk seems to be a disruptive and dangerous source of PD phenomena. Another type of discharge that occurs in dielectrics is known as 'treeing discharge', so named because of its branched tree expansion path (Figure 1b). Different types of electrical trees exist, such as branch types, bush types, dendrites, spikes, bow ties, and vented trees. They can occur due to high divergent electric stress over a long period of time, initiated from mechanical defects (e.g., protrusions, cracks, physical sharp points, imperfections, etc.), gas voids, or impurities within the insulation materials. Recurring faults will cause the electrical trees to spread and lengthen due to the decomposition of organic substances forming the bulk dielectric, which will then degrade its insulating capability. Thus, electrical trees have long been considered a significant insulation hazard that, if triggered, results in a full discharge [32]. Surface discharges occur on the surface of any solid insulating material under the tangential components of the electric field (Figure 1c). This discharge, identified by crackling and the smell of ozone, is commonly seen on overhead line insulators, especially contaminated insulators, during days of high humidity. Corona discharges (CDs) occur under high voltage stress when a conductor has sharp irregularities and is exposed to air. At these sharp points, a strong enough electric field is created and causes the ionization of the air, which conducts electricity and ignites an electric arc, corroding the insulation (Figure 1d) [8,33]. Unlike other types of PD, a corona discharge is visible and usually revealed by a relatively steady glow or brush discharge in the air. Corona PD is what we often hear in outdoor switchyards, particularly when the weather is humid, and it is usually not harmful.

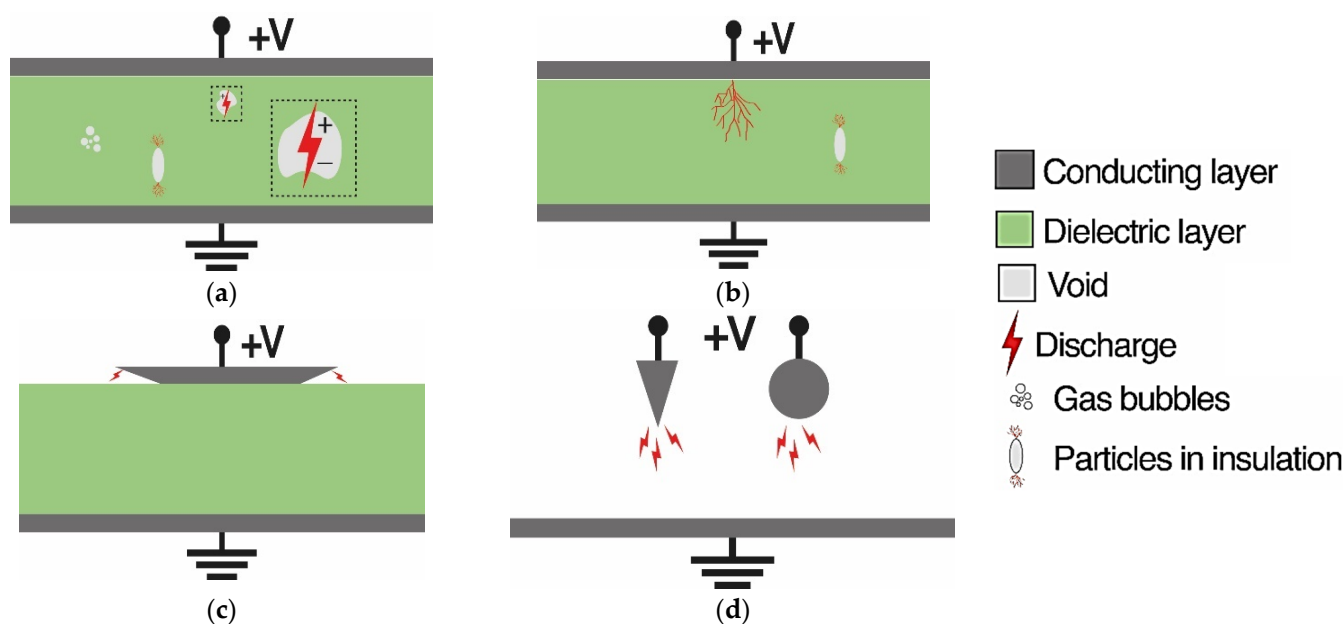


**Figure 1.** Different types of partial discharges: (a) internal, (b) treeing, (c) surface, and (d) corona.

## 2.2. PD Patterns Representation

The processing of PD-related information includes three main steps: detection, classification, of which recognition is an important part, and finally, localization. In 1961, Kreuger was the first to deal with the identification of the PD phenomena [34], followed by Gulski's work on their recognition in 1991 [35] and their classification in 1993 [10]. Discharges of unknown origin can be recognized via the classification process by matching the fingerprint of the examined discharge with known patterns. As such, differentiating between diverse types of PDs provides an initial assessment of the nature and severity of the deteriorated spot where the PD is occurring to facilitate grid diagnosis operations and reduce maintenance time [12]. Recognition of PD defects (including corona, internal, poor contact, floating metal work, etc.) can be performed with two basic implementation approaches: time-resolved or phase-resolved patterns; each has advantages and challenges. The time-resolved pattern, or  $q-t$ , is the signal output waveform  $q$  (where  $q$  is the amplitude of either the apparent charge in pC or the voltage pulse—discharge voltage—in mV) captured by the sensor versus time,  $t$ . This individual PD pulse shape may be of interest in time-resolved data patterns since there is a link between the PD signal shape and the type of insulation defect, which offers aging information about the insulation system [10,36]. The phase-resolved PD (PRPD) pattern is a visual representation of PD activities relative to the 360 degrees of an AC cycle. The HV AC test voltage waveform is used as a reference for gathering PRPD data, which is frequently referred to by  $\varphi-q-n$ . In the phase-resolved recognition method, a strong relationship is found between the shape and type of PD pattern, but it is independent of the electrical path between the defect and the detector [37]. Practically, a PD detector is required to pick up the individual PD signal and measure all pulse occurrences over a given duration based on the phase angle ( $\varphi$ ), discharge magnitude ( $q$ ), and discharge rate (or number of PDs,  $n$ ), at a specified test voltage [38]. For computational purposes, the relevant phase and amplitude pulse numbers of PRPD patterns are often kept in matrix format [36]. The data analysis module is often equipped with advanced pattern recognition techniques to help differentiate PD from noise and even to identify the specific sources of PD and locate them. However, in the time-resolved method, a strong relationship between the physics of the defects and the shape of the signal is found [37]. When compared to phase-resolved measurements, time-resolved patterns often require less costly measurement apparatus. Phase-resolved data are commonly utilized in PD classification studies because they can describe the physical operation process at

the PD location, as individual PD pulses have a strong relationship to PRPD patterns. Figure 2 depicts typical PRPD representative patterns for each defect type. These results were recorded using an HFCT sensor, according to Romano et al. [39].

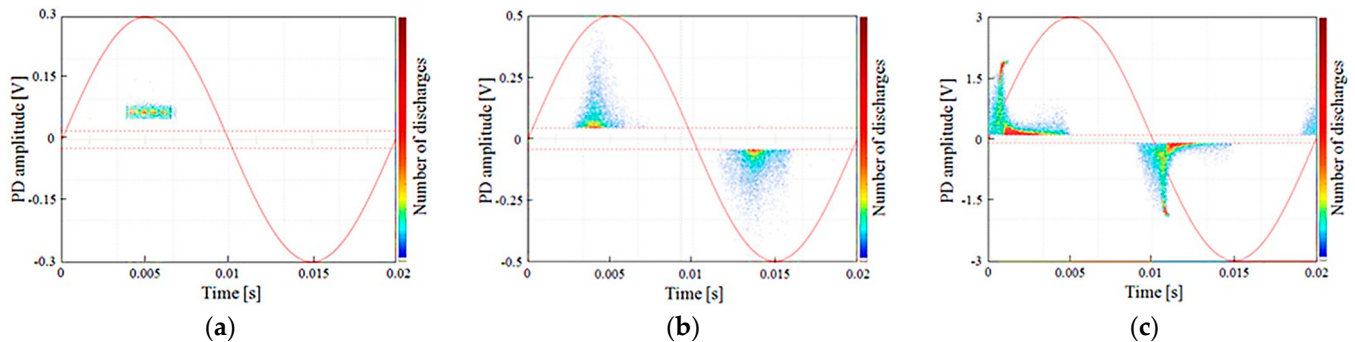


**Figure 2.** PRPD patterns (colored points) showing the magnitude of all recorded discharge events ( $y$ -axis) plotted against time ( $x$ -axis) compared to the excitation AC for: (a) corona discharge, (b) surface discharge, and (c) internal discharge [39].

Kreuger's method [10,34] served as the foundation for the development of other various diagnostic and recognition techniques for PD, most of which are based on neural networks [40], fuzzy logic [13], and more or less complicated statistical approaches [41]. Statistical techniques are based on studying a single PD, analyzing and removing noise (caused by several sources, including radio masts and DC light fittings) in order to better understand the discharge characteristics. Following this, several statistical studies were carried out, referring to the polarity of the PD current pulse, its magnitude, the distribution of the pulses and their number, and the characteristics related to the phase angle of the PD trigger, as well as the phase difference between the beginning and end of the discharge [42–44].

### 2.3. Offline Versus Online Measurement

Offline and online PD detections are the two basic ways of measuring PD. Offline procedures are tests in which the equipment under inspection is disconnected from regular operation and powered by an external voltage source [45]. Since the applied measurement voltage may be varied, offline PD testing offers advantages, such as the ability to calculate PD extinction voltage (PDEV) and PD inception voltage (PDIV). Online testing is carried out while the equipment is powered up at the recommended operating voltage, allowing accurate PD behavior to be acquired and assessed (real operating conditions are applied). The benefits of online PD testing include PD characteristics that may be measured under varied load circumstances and the ability to conduct tests without causing a power interruption. Now only offline procedures are standardized in IEC 60270. Online approaches continue to be novel, with no standard to compare them against. On the other hand, in recent years, online tests have gained popularity for diagnosing PD in cables. Indeed, current online detection and localization techniques can locate PD sources in switching and cabling equipment, thereby reducing the downtime needed to repair or replace assets. Online and offline PD testing complement each other. A more accurate assessment of cable condition can be achieved by combining both approaches. The majority of PD classification research employs the offline detection approach, as it is more convenient to undertake in a lab setting.

### 2.4. Different Methods for PD Detection

Several methods have been developed over the years, both offline and online, to detect and locate the presence of a PD based on the phenomena generated during the discharge defect. Most of these focus on wideband measurements using various types of sensors, different noise rejection techniques, pulse classification methods, and defect location and identification possibilities [46]. Table 1 describes the various PD detection techniques based

on physical characteristics, such as the electrical discharge current impulses based on the IEC 60270 standard, by-products of chemical reactions, acoustic emissions (pressure waves), and electromagnetic (EM) waves or electromagnetic interference (EMI) emitted in different frequency ranges (HF, VHF, UHF, light). A brief introduction to the principle of each method as well as the sensor used will be presented thereafter.

**Table 1.** Most common partial discharge detection methods.

Method	Detection Phenomena	Applied Sensor	PD Localization	Online Monitoring
Electrical method	Compensation current due to dielectric loss (current pulse from kHz to some MHz)	Coupling capacitor (IEC 60270) [47] Transient earth voltage (TEV) [48]	Yes	No
Chemical method	Change of gas pressure Chemical change	Gas chromatographs High-performance liquid chromatography (HPLC) Dissolved gas analysis (DGA) [49]	No	Yes
Acoustic method	Mechanical pressure waves (sound)	Ultrasonic microphone (with 40 kHz center frequency) Piezoelectric sensors [50] Acoustic contact sensor (with detection bandwidth range 20 kHz–300 kHz)	Yes	Yes
Electromagnetic method	Electromagnetic interference (EMI) detection (high-frequency waves)	VHF/UHF antennas [51] Radio/high-frequency current transformer (RFCT/HFCT) [52] Inductive loop sensors [53]	Yes	Yes
Optical method	Optical effects (ultraviolet—visible—infrared range)	Mach–Zehnder fiber interferometers/Fabry–Perot interferometers [54] Infrared camera [55]	Yes	Yes
Thermal method	Heat/high temperature	Resistance-temperature sensor (RTD) [56]	No	Yes

#### 2.4.1. Conventional Detection Method: IEC 60270

Electrical detection of PD relies on sensing the high-frequency current pulse that travels through the object's insulating capacitance due to a flashover occurrence. The electrical method based on a coupling capacitor for PD detection as described in the IEC 60270 standard is widely established due to its accuracy and ability to detect PD levels under offline conditions. Figure 3 depicts the test circuit used for PD measurements in this approach, which consists of an HV AC source with a sufficiently low level of background noise, the test object  $C_x$  (in which the PD occurs), a coupling capacitor  $C_b$  (with low inductance design), and a measuring impedance  $Z_m$ , as important circuit components. The filter unit  $Z_e$  suppresses unwanted high-frequency background noise or disturbances generated by AC voltage sources. It is usually built as a large inductor because the tested object insulation system,  $C_x$ , exhibits a predominantly capacitive character. The coupling capacitor, when connected in series with the impedance  $Z_m$ , creates a capacitive divider, converting the high-frequency current into a voltage signal detectable by the measuring instrument [57]. When a discharge occurs in the object under test, the coupling capacitor transfers a charge to it to compensate for the momentary collapse of the voltage across it [18]. As a result, when coupling the sense impedance  $Z_m$ , the sub-1 MHz current pulse resulting from PD activity in the test object ( $C_x$ ) can also be detected from the coupling capacitor branch. The coupling device serves as a measuring module from which the PD voltage signal can be extracted. Such an approach provides additional information about the test voltage, which is needed for a phase-related partial discharge (PRPD) measurement. The

signal can be represented in both time and phase domains to illustrate the characteristics of the PD events. The test configuration shown in Figure 3 is appropriate for measuring PD from a test object that has a ground terminal or is connected between the HV AC source and the ground [18]. The coupling capacitor picks up and detects the PD-generated current at the test object, which has a connecting loop to the ground line through some impedance. When a discharge occurs, a transient current flows in some ns in the external circuit  $Z_m$  corresponding to an amount of charge (known as the apparent charge). This pulse can be measured using the impedance  $Z_m$ , often composed by a parallel RLC circuit. The inductance  $L$  strongly attenuates the low-frequency components of the measured signal, the capacitance  $C$  incorporates rapid PD pulses, and the resistance  $R$  dampens the voltage oscillations at its terminals. After calibration, this circuit measures a signal proportional to the apparent PD. Electrical measurement provides high sensitivity and is easy to execute. However, due to its high sensitivity, it is prone to problems and therefore unsuitable for the long-term monitoring of transformers.

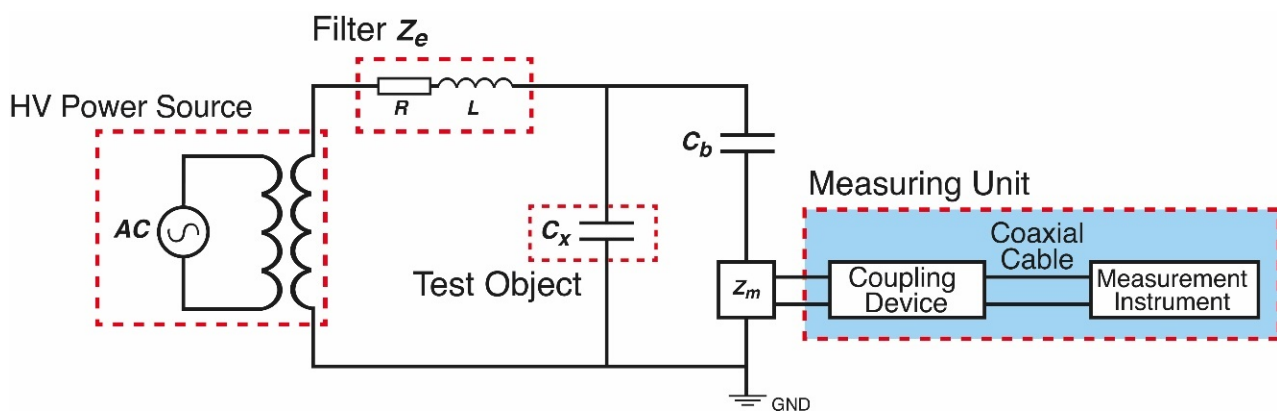


**Figure 3.** Electrical PD measuring circuit based on the IEC 60270 standard.

#### 2.4.2. Radiofrequency (RF) Methods

The RF approach utilizes appropriate sensors to detect and receive the electromagnetic wave generated when PD occurs. The emitted EM radiation consists of a combination of different frequency components up to a few GHz, which are classified into three bands: high-frequency (HF), very high-frequency (VHF), and ultra-high-frequency (UHF) [58]. RF-based techniques to detect PD activity have interesting characteristics because they allow noninvasive, continuous, and low-cost monitoring of PD activity. Moreover, among the various PD detection methods, they have the advantage of supporting online monitoring and allowing defect classification. Since EM waves in space consist of an electric field measured in V/m and a magnetic field measured in A/m, by using a loop antenna, the magnetic field perpendicular to the electric field can be detected separately. On the other hand, since the PD causes a high-current pulse to travel along the shield to the ground strap, inductive sensors, based on Faraday's law of induction, are also used to measure changes in the magnetic field surrounding the ground line caused by the PD pulse. Hence, several types of sensors can be used for EM wave detection, such as UHF/VHF antennas [51], inductive sensors [59], or loop antennas [60]. The high-frequency current transformer (HFCT) is an inductive sensor clamped over the ground terminal of the HV equipment that may measure HF signals (3–30 MHz). However, the result can only suggest the presence of PD defects without pinpointing their precise position. On the other hand, the UHF method is widely used for online monitoring of PD sources due to its noise immunity and localization efficiency [61]. The UHF method has a high signal-to-noise ratio thanks to its measurement frequency range of 300 MHz–3 GHz [10], which is superior to electromagnetic interference from corona discharge in the surrounding environment. Various RF approaches have been studied, developed, and applied to PD measurement, location, and processing techniques for different configurations in order to obtain precise diagnoses [46].

### 2.4.3. Non-Electrical Methods

Besides RF detection, other unconventional methods rely on other physical phenomena associated with PD events, such as light waves, chemical by-products, acoustic signals, local temperature rises, etc. Optical sensing is undertaken by placing an optical sensor close to the power equipment. It is based on the detection of light generated as a result of the ionization, excitation, and recombination processes that take place during the discharge. However, the optical spectrum of various discharge types is not the same. The insulating medium (gaseous, liquid, or solid) and other factors (temperature, pressure, etc.) affect the amount of light emitted and its wavelength. As a result, the surrounding medium and the intensity of the discharge affect the spectrum of light emitted by PD. The optical spectrum extends from ultraviolet in the visible range to infrared (Figure 4) [62]. The competitive advantage of this method is its immunity to electromagnetic interference (EMI). However, a significant limitation is its low sensitivity, which is excessively affected by internal barriers within the equipment, which causes light reflection, scattering, and attenuation [8]. Another drawback is the high cost of optical sensors, which still requires improvement.

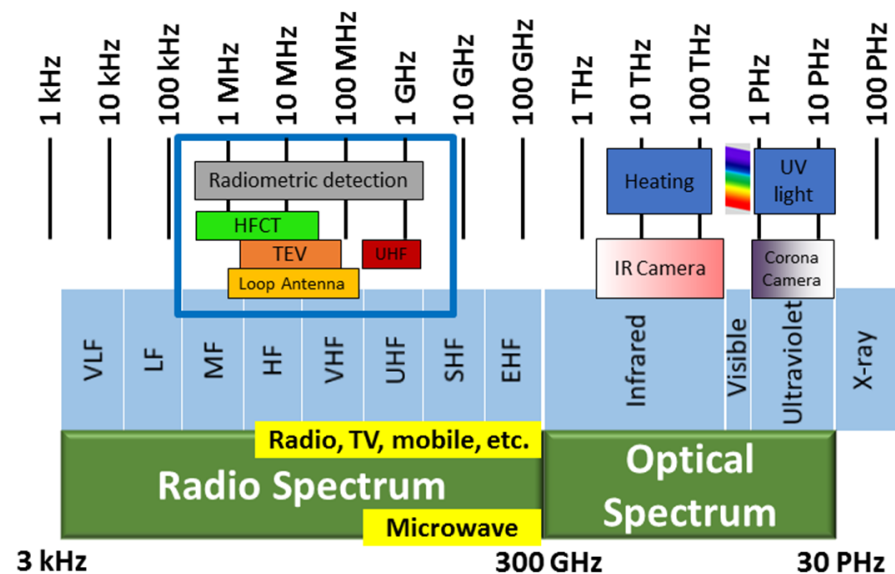


**Figure 4.** Location of the different radio and optical detection methods on the electromagnetic spectrum.

In the air, PDs generate gases such as ozone ( $O_3$ ), nitric oxide (NO), and nitrous oxide ( $N_2O$ ), which in turn yield nitrogen dioxide ( $NO_2$ ), and therefore nitric acid ( $HNO_3$ ) if water vapor is present. These toxic gases are corrosive and can degrade and weaken the insulation, in addition to causing shortness of breath in people. The chemical measuring techniques used to identify PD in high-voltage transformers are based on the collection and chemical analysis of oil and gas samples emitted during the PD process. Essentially, two chemical measuring procedures are in use: dissolved gas analysis (DGA) and the high-performance liquid chromatography (HPLC) method. HPLC analyzes PD-ejected by-products, such as deteriorated forms of glucose caused by insulation breakdown, whereas DGA analyzes the total amount of gas generated by the PD [29]. Before chemical testing techniques can be used, sufficient by-products or ejected gas must be collected. Therefore, there will be a time lag between the collection and analysis of data, which makes chemical detection unsuitable for real-time monitoring. Furthermore, both methods are not able to provide information about PD localization [49,63].

Acoustic emission (AE) is frequently involved during the discharge process, and the emission measurement frequency band is 20 kHz to 1 MHz (from audible to ultrasonic). This sound is created when a streamer discharge is formed and the material surrounding it is vaporized, causing a rapid release of mechanical energy that propagates in the form of a pressure field. The acoustic method is widely used for online PD detection due to



several advantages, such as being less sensitive to electromagnetic interference and having the ability to precisely locate the discharge. The acoustic method can detect multiple PD sources [64]. To overcome the incapability of detecting the PD level and calibration, the AE method is combined with other methods such as optical, UHF, and electrical detection. The drawbacks of this method are the complex behavior of the acoustic emission, the low intensity of the detected signals, and the high cost. Many types of acoustic sensing devices are in use, such as condenser microphones [65], piezoelectric transducers [66], accelerometers [67], and fiber optic (FO) sensors [64].

In order to improve cost-effectiveness and anti-electromagnetic interference capability, optical fiber acoustic sensing technology has been introduced by merging optical and acoustic methods. The synergistic combination of these two methods makes it possible to obtain high precision in locating the insulation fault while reducing the time of the measurement procedure. The sensing principle of an intrinsic fiber optic acoustic sensor is based on the change in the length of the optical path produced by the strain induced by the acoustic pressure waves [68]. Pulse-current and UHF detection methods are mature technologies with high sensitivity but poor performance when used in harsh electromagnetic field environments with large temperature changes. Nowadays, fiber optic acoustic sensors have become very attractive research subjects for PD detection thanks to their good sensitivity, immunity to electromagnetic interference, and electrical non-conductivity [54]. The optical detecting technology is functionally based on fiber optic intrinsic interferometers (like the Michelson interference sensing system, Mach–Zehnder interferometers, and multimode fiber [69]) and fiber optic extrinsic interferometers (like Fabry–Perot interferometric sensors) [54]. Interferometers based on optical fibers are a type of phase-modulation ultrasonic sensor, and their response performance is closely related to the initial phase position.

PD detection using thermal sensing is usually achieved by placing a resistance temperature detector (RTD) or a thermocouple next to suspicious equipment parts [70]. RTDs consist of a metallic resistor with a high temperature coefficient (such as platinum, nickel, or copper), which changes resistance in proportion to the change in its temperature. The current is passed through a resistive element (mostly a metal film with a serpentine path), and the voltage is measured across the same element to determine the resistance and hence the temperature. In higher-quality RTDs, such as those used in large rotating machinery, the leads may be contained within a grounded metal shield to reduce electrical interference, thereby improving temperature sensing [70]. Two-wire detectors suffer from an inherent inaccuracy due to the lead wire resistance, which will cause an offset increase in the resistance measurement. The three- or four-terminal devices are built with a compensation loop to allow the measurement to subtract the lead resistance. Lead lengths from the sensors to the terminal panel can vary significantly from one RTD to another, even within the same stator. Indeed, RTD leads in motors can be only a meter long, whereas those in large generators can be 10 to 15 m long.

In the next section, we focus on the detection of PD using the released high-frequency electromagnetic fields in different frequency ranges (HF, VHF, and UHF), as shown in Figure 4.

### 3. Radiometric Sensors for PD Detection

The RF method was developed in 1988 to record the EM waves radiated from the PD source for gas-insulated switchgear (GIS) [71] and was subsequently adapted to power transformers and cables in 1997 and 1998 [72]. The PD rise time of the pulses (as low as a few ns) indicates that they have a wide frequency spectrum that can reach up to several hundred MHz or even the GHz range. Hence, the RF signal created by PD activity could fall within many RF frequency bands (HF, VHF, and UHF). The main advantage of these types of sensors is that they do not require galvanic contact with the equipment to be monitored. With the proper calibration, observed PD signals may be utilized to diagnose the insulation status of the GIS, transformers, and cables. Online PD measurement is one of the main advantages of the radiometric technique. In the next section, various types of radiometric

sensors operating in different frequency bands are presented and discussed. Thereafter, radiometric sensors will be divided mainly into three categories: inductive sensors, loop antennas, and VHF/UHF antennas, depending on the electromagnetic wave component detected (B- or E-field) and the detection location, either from the free space or from the ground cable.

### 3.1. Inductive Sensors

Inductive sensors, which are suitable for detecting the PD mainly in the HF band, are detailed afterward.

#### 3.1.1. High-Frequency Current Transformer (HFCT)

The HFCT sensor is a high-frequency current transformer designed specifically for picking up partial discharge signals, predominantly in power cables. It consists mainly of an electrical wire (the secondary) wound around a toroidal, soft ferrite core (Figure 5a). The toroid is clamped around the earth sheath (the primary), through which pulse-shaped noise interferences (PD pulses) pass (Figure 5b). This transient current signal in the power cable excites a magnetic field that will be concentrated and confined in the toroidal core. This magnetic flux induces a corresponding voltage in the secondary winding of the HFCT, which can be measured at the output of the sensor [73].

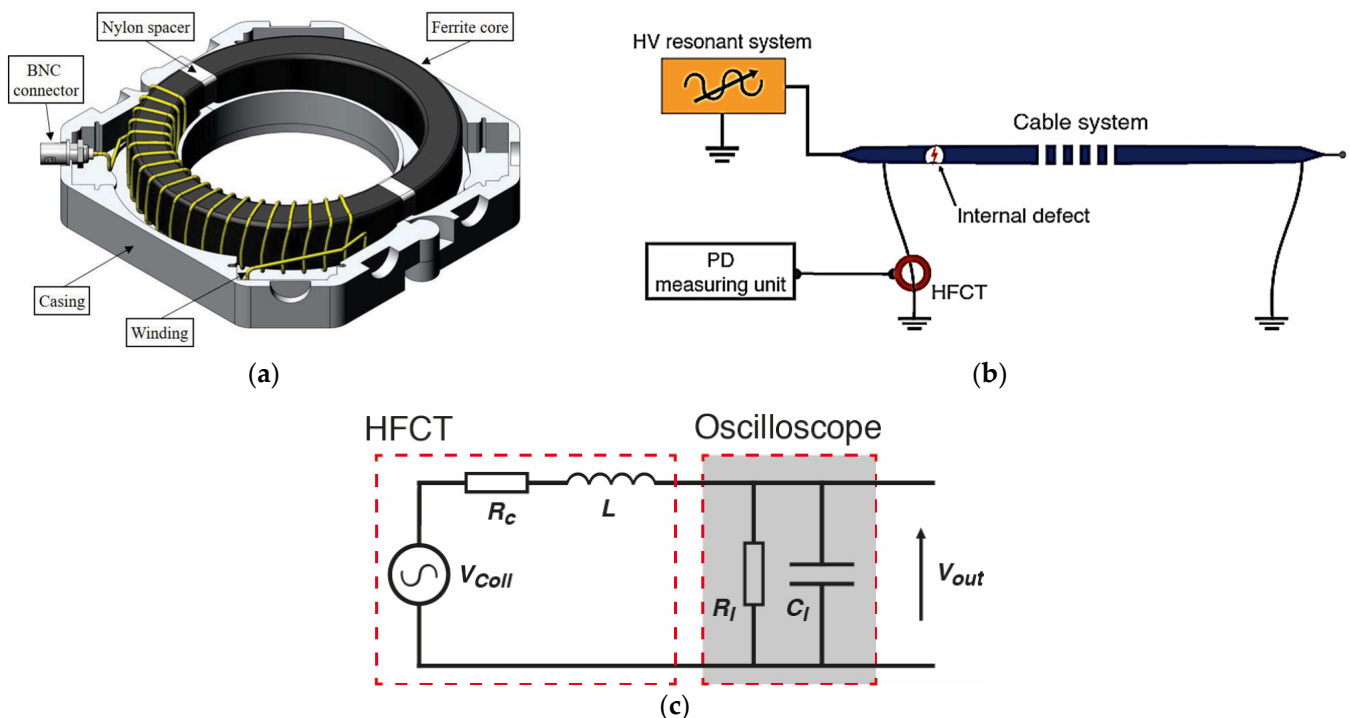


**Figure 5.** (a) HFCT model (20 winding turns) with the top part of the casing removed [74], (b) HFCT sensor placed in a ground conductor for PD measurement in the cable system, (c) the equivalent circuit model of the HFCT sensor.

HFCT sensors often have a ferrite split core, which makes them easy to install and allows them to be retrofitted to earth straps without disconnection. The measuring frequency range for this type of sensor is 30 kHz–30 MHz, which covers the HF band. Indeed, ferrite cores are widely accessible in the required frequency range, making the production of high-quality HFCT sensors simple and affordable. Certainly, a higher cutoff frequency would ensure faithful rendering of fast transients. The equivalent circuit model of the sensor is illustrated in Figure 5c. The sensor may be described as a system, with the input

being the current of the PD pulse  $i$  flowing through it and the output being the induced voltage. The transfer function can be expressed as:

$$e = M \frac{di}{dt} \quad (1)$$

where  $M$  is the proportional constant or the mutual link between the earth conductor and the secondary winding. From this equation, it can be noted that the voltage induced in the secondary is proportional to the rate of change of the current in the primary. HFCT sensors make it possible to provide a very precise, non-contact, and non-destructive measurement of a single or repetitive bipolar or unipolar pulse. Additionally, since the coupling between the sensor and DUT is inductive and therefore galvanically isolated, HFCT sensors are well suited for online monitoring.

Online HFCT's capability to locate and identify dangerous PD activity in rotating machines, cables, switchgears, and transformers has been confirmed [75]. The severity of the PD is quantified by measuring the burst interval between the end of a burst and the beginning of the next burst. As the insulation failure worsens, the burst interval shortens until the critical point of two milliseconds is reached, resulting in a major failure with full-blown discharge. Current pulses created near the discharge's origin have risen times of nanoseconds or less, producing a frequency spectrum with substantial components down to hundreds of MHz or even units of GHz [76]. PD detection with HFCT sensors has several advantages, including: (i) sensitivity is not as dependent on pulse shape as in traditional PD measurement equipment; (ii) data evaluation in certain frequency bands and signal-to-noise ratio (SNR) can be enhanced; and (iii) sensitivity is high when the sensor is close to the PD source and low when far from it. In addition, when two or more HFCT sensors are installed in an HV installation, measuring PD pulses with a common time reference allows fault locations to be determined using time-of-flight analysis [75]. The use of an HFCT sensor as a phase-resolved PD detector is constrained by certain factors, such as its sensitivity to reading low PD amplitudes, its response time to avoid interference during successive readings, and its sampling frequency to detect enough PDs in one AC voltage cycle (20 ms for 50 Hz). The collected signals can be categorized by analyzing the pulse shape in order to distinguish between various PD types or noise sources. A precise categorization of recorded pulses, followed by an examination of associated PRPD patterns, improves the sensitivity of flaw detection and enables more accurate diagnoses. Finally, when a PD pulse propagates through the cable shield in a power cable system, the pulse may be monitored at distances exceeding one kilometer while maintaining spectral content up to units of megahertz [75].

### 3.1.2. Rogowski Coil (RC)

HFCT sensors are excellent for measuring PD pulses but are made of expensive ferromagnetic materials, which can become saturated when coupled to high voltage wires on one side, and can handle up to 50 MHz in flux lines on the other. As an alternative, the Rogowski coil (RC), named after Walter Rogowski, is an electrical device that has been employed for around a century for measuring alternating and impulse currents. It consists of a helical coil, of which the wire from one end returns through the center of the helical to join the first end so that the two terminals of the coil are at the same side (Figure 6) [21,77]. RC is similar to HFCT but without a magnetic core; hence the term "air-cored coil". Depending on the type of construction, the smallest currents with rise times in the nanosecond range or the largest power-frequency short-circuit currents can be measured. The coil is constructed using a helical winding wound on a non-magnetic toroidal solid core. The return wire is passed through the torus to have both ends on the same side for even easier installation rather than a split-core current transformer and to cancel out unnecessary electromagnetic fields. Indeed, any axial magnetic flux will induce voltages in both the central conductor and the helical winding turns. If the diameter of the toroidal winding is small enough compared to the major torus diameter, the induced voltages from the two

wires will oppose and cancel each other out. In contrast, a radial flux will not produce any voltage in the central conductor. Toroidal windings, with a relatively large pitch, can induce significant voltage. However, the radial flux must intersect these turns in the positive and negative directions, so the induced voltages almost cancel each other out. Consequently, only azimuthal magnetic flux induces significant voltages in an RC. The RC sensor operates with the same principle (Faraday's law) as the HFCT sensor, so it senses the time derivative of the current pulses associated with PD and produces a proportional output. This variable current creates a magnetic field that connects the secondary of the coil and causes a voltage that is directly proportional to the current change in the conductor as well as the mutual inductance between the coil and the conductor [78]. Often, a passive integrator used with a Rogowski coil can provide an output signal proportional to the current passing through the toroidal opening. Common integration methods are active integration with operational amplifiers and passive integration with resistive-capacitive circuits [79]. The RC sensor has a linear characteristic due to the absence of magnetic materials. It has some notable characteristics that have attracted attention in recent years, including: (i) withstanding large overloads without damage; (ii) measuring currents over a wide range, without saturation; (iii) being easy to use, due to its flexibility and lightness; (iv) low cost; (v) non-intrusive nature (drawing no power from the main circuit); (vi) wide bandwidth, in the range of 0.1 Hz to 1 GHz (HF and VHF bands); and (vii) excellent transient response and safety (electrically isolated from the main circuit) [80]. Aside from this, RC can be influenced by nearby conductors carrying high currents because it utilizes a non-magnetic core to support the secondary windings, resulting in a weak mutual coupling between the primary and secondary windings. Due to this issue, identifying the proper number of RC turns should be one of the solutions to determining and optimizing sensitivity. A higher number of turns causes an increase in inductance, which in turn will decrease the resonant frequency. The RC is designed for PD detection and measurement at high frequencies ranging from tens to hundreds of MHz.

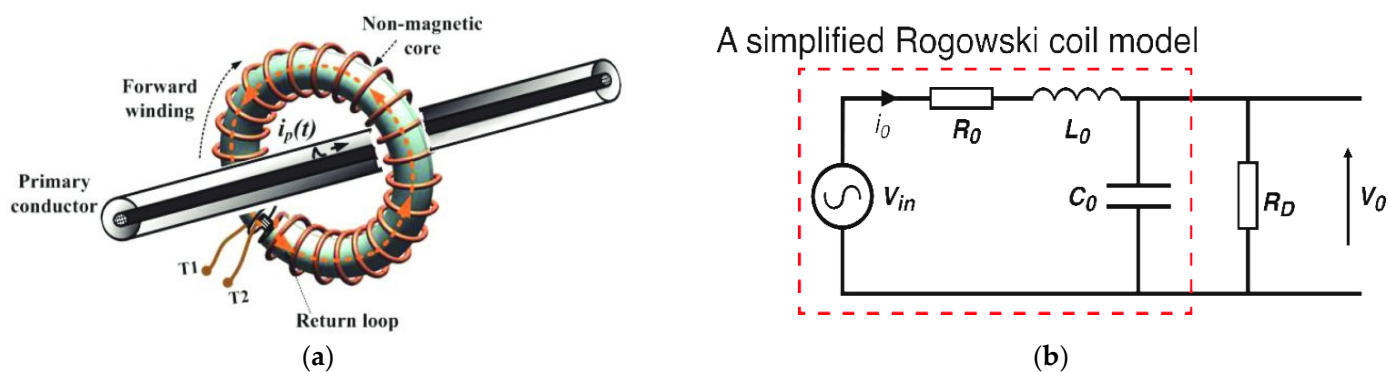


**Figure 6.** (a) principle of the Rogowski coil for measurement of nanosecond-rise time pulsed current [77], and (b) lumped equivalent model of a Rogowski coil [81].

Kumar et al. [82] proposed a simple construction of two low-cost air-core RC sensors to measure the PD pulse current by investigating the effect of winding turns. The results showed that Design 1, with 30 turns, has an operating frequency of 375.19 MHz and bandwidth coverage up to 32.28 MHz, while Design 2, with 60 turns, has an operating frequency of 510 MHz and a bandwidth coverage of only 17.14 MHz. The RC sensors' experimental performances were compared to those of a commercial ferrite-core HFCT having an operating frequency of 123.24 MHz and a bandwidth of 257.87 kHz. The three sensors were used to detect three types of discharges, namely streamers in mineral oil, trees in silicone rubber, and vacuums in pressboard. Experimental results showed that the manufactured RC with a higher turn number (Design 2) could detect the PD pulse with similar performance to the HFCT commercial sensor. This result was obtained with linear regression statistical methods, proving that the constructed RC had a linear relationship

with the HFCT sensor. Shafiq et al. [83] presented a lumped parameter identification of an RC sensor for internal PD detection based on an experiment methodology. The results obtained from the RC sensor, which had an operating resonance frequency of 37.6 MHz and a bandwidth of 0.5 to 80 MHz, were compared to those of a commercial HFCT sensor. Moreover, a simple and efficient digital integration technique was adopted to avoid the conventional types of costly and complex analog integrators. Laboratory tests revealed that the proposed RC sensor was suitable for PD detection; however, due to the lower number of turns, its output was not significantly responsive to electromagnetic interference, and more tests in a real online system are required [83]. Sharifinia et al. [84] dealt with a new high-efficiency printed circuit board (PCB)-based RC sensor for detecting and locating PD in power transformers. The sensor had a thin, flat shape and could be placed on the internal surface of the transformer tank. The sensor geometry was optimized to handle the trade-off between low resonant frequency and high mutual inductance. The results showed that the RC sensor operated in a frequency range of 10 Hz to 10 MHz. Herein, the authors performed a test of measuring PD in transformers for different positions and distances, and the accuracy of PD localization was studied. It was found that by increasing the distance of the RC sensor from the PD source location, its sensitivity decreased. Moreno et al. [79] proposed a Simulink model that anticipated the amplitude and phase of the PD pulses obtained in the laboratory thanks to an implementation of the RC lumped parameter model. They numerically studied the time and frequency responses of RCs with several turns, different dimensions, and different output impedances in order to give design guidelines for measuring high-frequency pulses. Waldi et al. [85] proposed a comparison between two different geometries of RCs to assess their PD detection capabilities. The first was without a back lead (Figure 7a), and the second was with a back lead (Figure 7b), with 5, 10, 20, and 40 turns. Test results showed that both sensors acted linearly toward the imitated PD pulse; however, as the number of turns increased, there was an increase in the response output of the measured wave in a nonlinear trend. Liu et al. [86] presented an improved lumped parameter model applicable over a wide frequency range to both double- and single-layer high-turn RCs. The influence of five major design factors on the linearity and output voltage of RC at different frequencies was investigated both theoretically and experimentally.

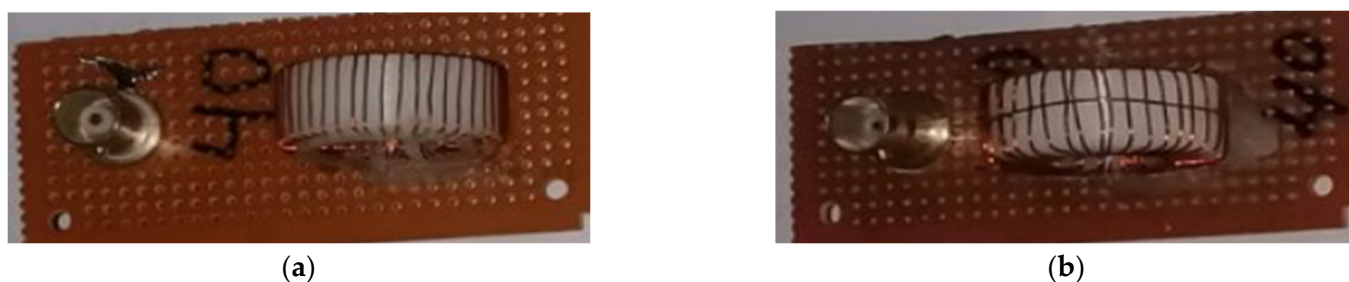


**Figure 7.** RC sensors with 40 turns tested in [85]: (a) without back wire, and (b) with back wire.

### 3.1.3. Inductive Loop Sensor (ILS)

An effective PD sensor should be compact and easy to install, sensitive to tens of pC of PD level, and have high saturation performance. Another simple, low-cost air-cored inductive coupling sensor capable of measuring PD pulses with simple distributed parameter models with high-frequency and high saturation performance can be used. The loop inductive sensor (ILS), consist of a single conductive rectangular loop printed on a circuit board and placed parallel to the line that conducts the PD pulse stream (in series with the coupling capacitor). Like HFCT and RC sensors, ILSs are based on Faraday's law and measure the voltage induced in a loop through the change in the magnetic field caused by the PD pulse. Hence, the magnetic flux through the surface of the loop induces a voltage proportional to the derivative of the primary current, which depends on the geometry of the turn and its separation from the primary conductor (Figure 8a). It has been

experimentally proven that these sensors are able to monitor various forms of PD from the ground line leakage current. The use of ILS sensors is very limited since a fixed separation distance of 1 mm from the primary conductor must be respected. This restricts the use of these sensors with real apparatus, such as generators and transformers, as there is no easy access to ensure galvanic coupling.

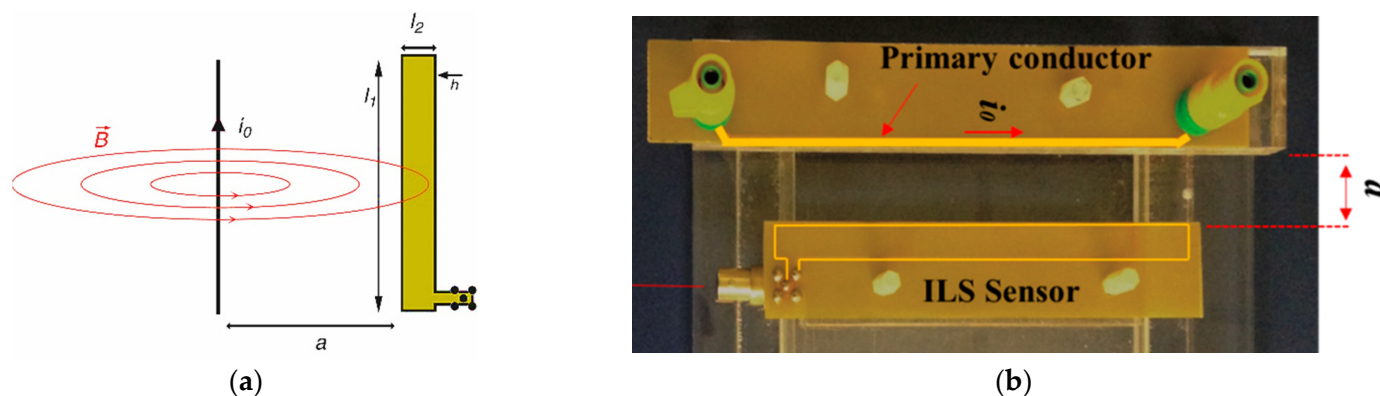


**Figure 8.** ILS sensor: (a) working principle based on Faraday's law, and (b) arrangement with the primary conductor carrying the PD pulse [87].

Robles et al. [59] tested the behavior of two ILS probes, with lengths of 6 and 12 cm, for PD measurements. The test specimen was a high-voltage transformer, and the separation distance from the measuring branch (the capacitive divider) was set to 1.02 mm. The amplitude of the signals given by both probes was compared to an HFCT sensor for known injected charge magnitudes from 10 to 100 pC. The authors highlighted that both ILSs allowed for measuring PD patterns and were compatible with modern recognition systems. Rojas-Moreno et al. [88] presented a self-integrating rectangular ILS by placing a specific resistor at its terminals in order to place a pole in the range of tens of megahertz. In fact, unlike RCs, which have significant capacitance, ILSs have a wide bandwidth because their capacitive effects are negligible, and thus, they do not present self-resonance. The sensor's empirical response was validated using a commercial HFCT, which determined its sensitivity and confirmed its performance as a valid inductive transducer with a bandwidth between units and tens of megahertz. Ardila-Rey et al. [87] designed an ILS on a PCB with a single turn (Figure 8b) having a cutoff frequency response of up to 45 MHz. The ILS sensor was used to detect PDs within a power transformer as a test object and was placed at different separation distances from the line through which the PD flowed (from 1 mm to 20 mm). The results confirmed that the laboratory experimental results were in good agreement with the real measurement and that the sensor was useful for PD detection.

Ardila-Rey et al. [89] presented a comparison of the three inductive sensors (i.e., HFCT, RC, and ILS) and evaluated their ability to identify and separate different types of partial discharge in the laboratory using the chromatic technique. The HFCT sensor had a bandwidth from 1 MHz to 80 MHz with a sensitivity of about 25 dB, while the RC sensor operated in the range of 9 MHz to 60 MHz and had a sensitivity of about 12 dB, and the ILS sensor exhibited a derivative behavior between 0 and 34.69 MHz with a sensitivity of 17.5 dB. Among the three different sensors, the RC had the lowest sensitivity. All three sensors operated in the HF and VHF bands. Figure 9 illustrates the experimental setup used by the authors for PD detection. The experimental result showed that the HFCT sensor proved to be more robust against external disturbances, while the ILS and RC sensors presented signals that were more difficult to separate using the chromatic technique [89].

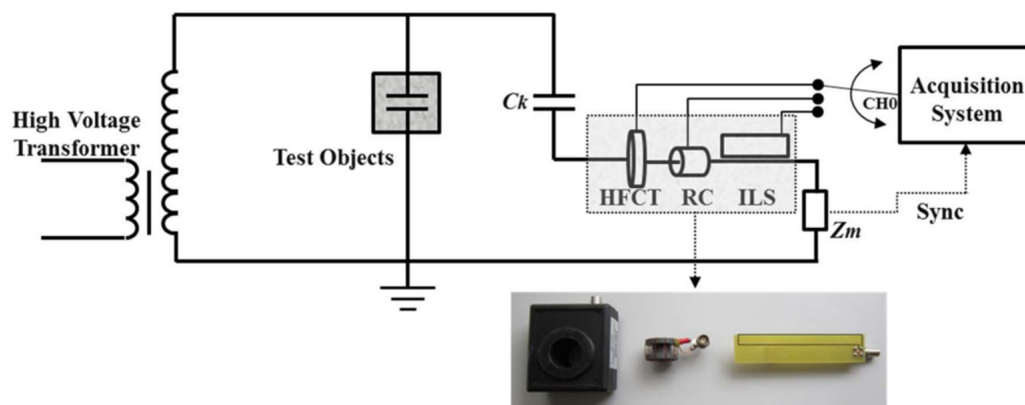


**Figure 9.** Experimental setup and location of the three sensors to record the partial discharge by [89].

### 3.2. Loop Antennas

Loop antennas, with one or more turns, are simple, compact, inexpensive, and versatile antennas with a wide range of applications. They consist of a closed loop, or coil of wire, of electrical conductors wrapped in a spiral or around a core. They may be in any shape, such as circular, rectangular, triangular, square, or hexagonal, according to the designer's convenience. Preferably, the loop should not meander in order to reduce its size, as this increases capacitive effects and results in low efficiency. Loop antennas pick up the magnetic component of an electromagnetic field in the HF band, unlike dipole antennas, which mainly respond to the electric component. Loop antennas are of two types: large loop antennas (or resonant antennas) and electrically small loop antennas (or magnetic antennas). The loop circumference of a resonant antenna is nearly equal to the signal wavelength to be measured. The circumference of the small loop antennas is well below the signal wavelength (in a ratio of a tenth up to a sixteenth) so that the current flowing through all the wires remains in phase. The characteristics of small loop antennas are: (i) low radiation resistance, which results in loss of power in the form of heat (this could be enhanced with a ferrite core), and (ii) low radiation efficiency due to high losses; hence, they perform better as receiving antennas at lower frequencies. Due to their closed design, loop antennas are primarily sensitive to the magnetic field and may function in near- or far-field situations depending on the circumstances [89]. According to Faraday's law of induction, the electromotive force induced in a receiving loop antenna is precisely proportional to the rate of change of magnetic flux over time across the loop surface. The sensitivity of the loop antenna is a function of the sensor's orientation. In electromagnetic waves, the magnetic and electric fields are transverse. Hence, if we place a loop oriented parallel to the direction of propagation, an electric voltage will be produced (the magnetic field will be perpendicular to the whole loop, see Figure 10a); if the loop is instead oriented orthogonally, there will be no magnetic flux, and therefore the voltage will be zero. The maximum radiation of a loop is off the vertical ends in a pattern similar to that of a dipole antenna (Figure 10b) [90]. Increasing the diameter/side of the loop antenna results in an increase in the radiation resistance and hence the efficiency. The effective area of a multi-turn loop is multiplied by the number of turns, as long as the loops remain small in comparison to the wavelength. Lastly, wrapping the loops around a ferrite core is a way to concentrate the magnetic flux in the loops and make them appear larger.

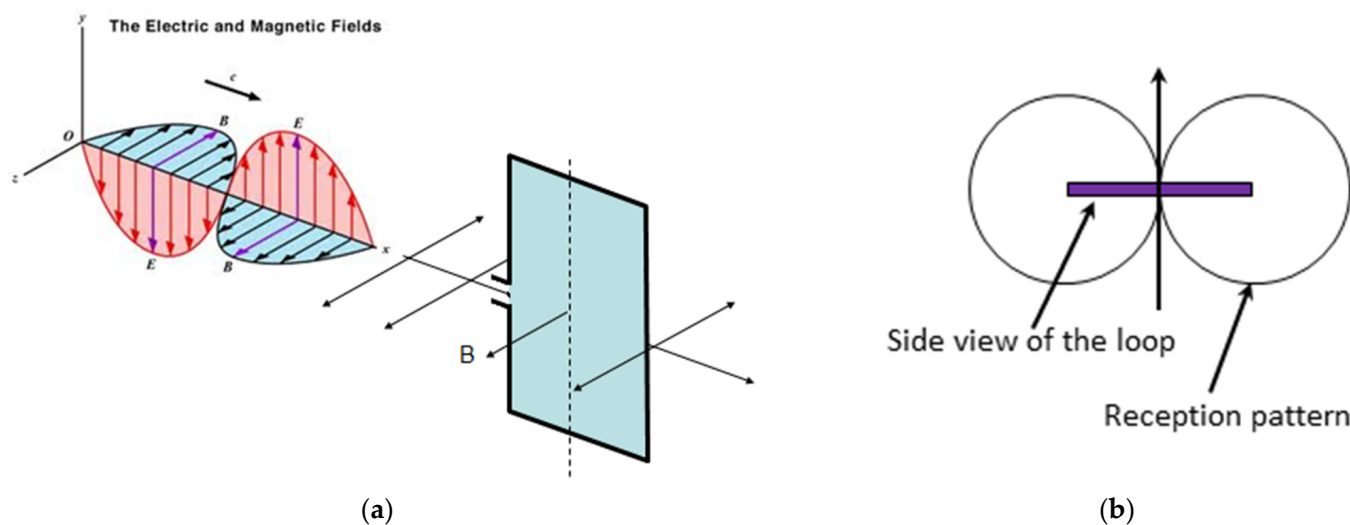


**Figure 10.** The magnetic loop antenna: (a) Best orientation and reception 2D pattern towards the emitted EM wave, and (b) reception 3D pattern in space.

Loop antennas, unlike ILS, do not need to be connected parallel to the ground wire to detect PD and can operate in free space close to the equipment to be monitored. Lopez-Roldan et al. [91] presented a first comparison review of antennas for PD applications in oil-filled transformers, including a small loop antenna with dimensions of 25 mm  $\times$  100 mm. The authors noticed that the loop antenna has less gain than the majority of the other tested types. Jin et al. [92] compared a 10-turn small loop antenna with an Mn-Zn ferrite core (relative permeability of 2000) and a diameter of 38 mm to a Hilbert fractal antenna. The loop antenna has a frequency pass band from 100 MHz to 700 MHz, while the other is from 500 MHz to 900 MHz. Both compact antennas are used for laboratory PD measurements of three typical transformer insulation faults, namely, cavity, surface, and corona discharges. The results demonstrated that both can be used effectively for PD online transformer monitoring. Rozi and Khayam [60] compared three single-turn small loop antenna shapes, namely, circular (Figure 11a), square, and triangular. The antenna circumferences were fixed at one-tenth of the induced PD wavelength, i.e., 30 cm, to achieve a bandwidth of 100 MHz. Time-resolved or phase-resolved patterns were measured when the antenna was placed 5 cm away from the PD source. The test results showed that the designed loop antennas were able to detect and measure PD with the superiority of circular shape. Widjaja et al. [93] discussed the optimization of a circle loop antenna as an online partial discharge (PD) sensor in a power apparatus. The sensor diameter was set at 9.55 cm to operate in the frequency range of up to 100 MHz. The effect of changing the number of turns (4, 7, 10, and 30) on the return loss, bandwidth, and voltage standing wave ratio (VSWR) were studied. The PD measurements showed that low sensor bandwidth led to a low amount of PD measured and that the optimum design of the loop antenna had 10 turns (Figure 11b). Hai-feng et al. [94] compared the performance of a multi-band resonant sensor (Figure 11c) based on loop antenna theory and meandering technique to that of a traditional broadband sensor. With the meandering technique, the limited length of the antenna could be extended, achieving lowered resonance frequencies and a minimized antenna size. Both devices were tested for three typical laboratory insulation defects (corona, surface, and free metal particle discharges). The multi-band circular antenna's working bandwidth was 480–520, 800–850, and 1100–1200 MHz, with a diameter of 5.2 cm. The results show that the multi-band sensor had higher detection sensitivity than a large-size broadband sensor, meeting the substation PD detection requirements. Zeidi et al. [95] presented the performance of a miniaturized on-chip loop antenna for PD detection with a side length of 1.8 mm (Figure 11d). The resonant frequency of the sensor was around 5 MHz. The latter was compared to the HFCT sensor and horn antenna for corona PD. The results showed



that the proposed magnetic antenna could detect PD when placed 15 cm away from a PD source with a 60 dB gain amplifier. The on-chip loop antenna had several advantages, especially in terms of reduced dimensions, and a lightweight, simple, compact structure, etc. Kaziz et al. [53] evaluated the performance of three 6-turn PCB-based inductive loop sensors for PD detection in power cables in a laboratory. The three square-shaped sensors, i.e., spiral, non-spiral, and meander, had, respectively, a side of 20 mm and a resonant frequency of 130, 1085, and 463 MHz. The test was carried out in three different positions: directly on the defective cable, at a separation distance of 10 cm to 3 m, and on the ground line. The experiment results showed that for the three positions, the non-spiral inductive sensor had the highest sensitivity for PD detection, while the meander sensor had the lowest. Furthermore, laboratory experiments have been carried out on the loop spiral antenna, showing its suitability for the detection of the three types of PDs, namely, corona, internal, and surface [53].

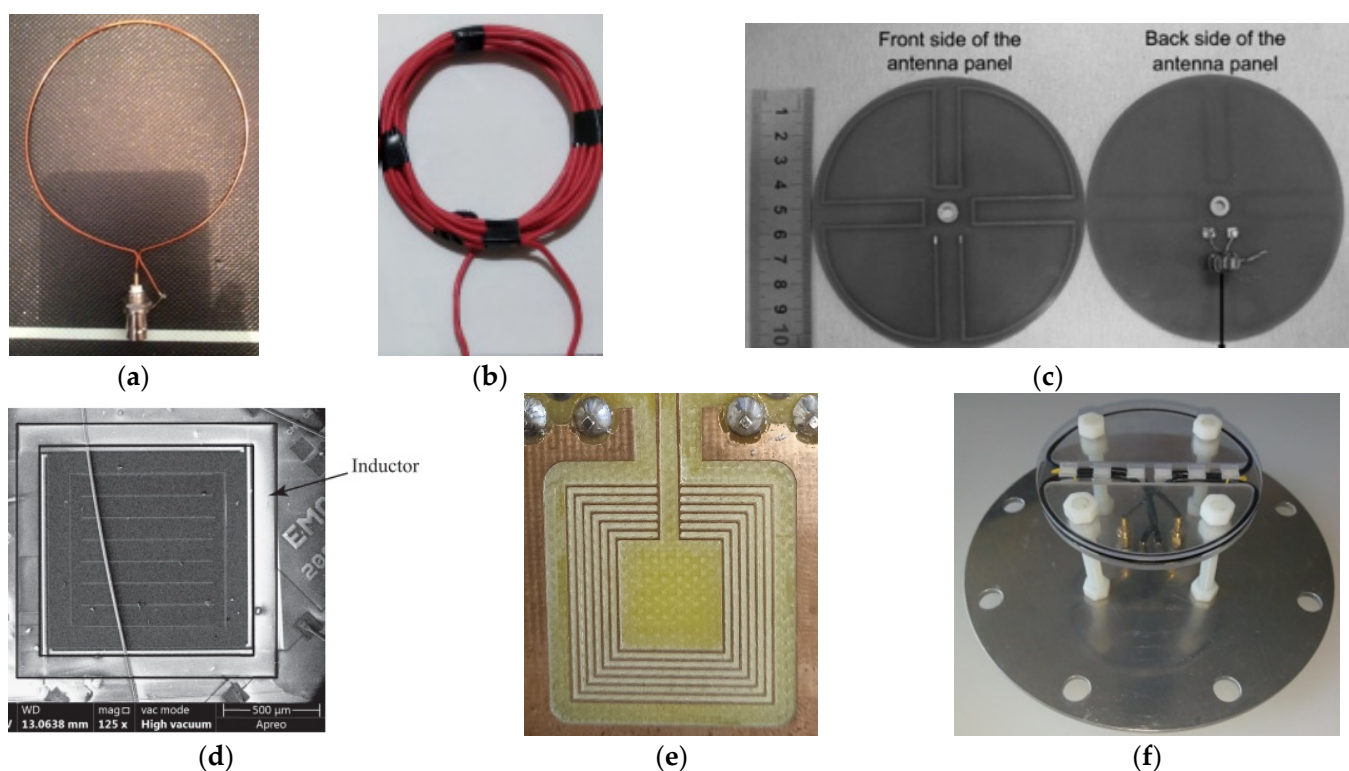


**Figure 11.** Loop antennas designed for PD detecting by: (a) circular loop antenna [60], (b) multi-turn circular loop antenna [93], (c) antenna panel [95], (d) on-chip integrated spiral antenna [95], (e) PCB-based non-spiral inductive sensor [58], and (f) single turn magnetic loop antenna [96].

Loop antennas can be categorized according to whether they pick up the EM signal from the air (free space) and function as a conventional receiving antenna in a communication system or capture it in a cavity. Mor et al. [96] presented a magnetic loop antenna for PD measurements on gas-insulated systems (GIS). The antenna was based on a shielded loop inserted in the dielectric window of a GIS, which measured PD currents propagating in TEM mode. The magnetic antennas were placed in the dielectric windows in such a way that a current signal traveling inside the GIS in the TEM mode caused a symmetric response in the two magnetic antenna loops [97]. This new measuring system was capable of estimating the PD apparent charge and detecting PD pulses below 5 pC. The antenna consisted of two shielded coils, each composed of a 5-turn loop wound in a half-circle shape [97]. During the experiment, the magnetic loop antenna (with a resonance frequency of around 32 MHz) was placed in two different positions in the GIS to detect three types of PD: corona, surface, and free-moving particles. When compared to the HFCT sensor, the results showed that the antenna could detect PDs in the HF/VHF bands with weaker

sensitivity. The article describes both the relevant parameters and the performance of the antenna in combination with a transimpedance amplifier.

Hussain et al. [98] discussed a comparative study between an RC, high-frequency E-field sensor (D-dot sensor), and a loop antenna. The sensors were tested to detect three types of PD (corona, surface, and internal) in a commercial switchgear panel. The proposed ILS showed the highest sensitivity compared to HFCT when detecting corona PD EM waves, but it presented lower sensitivity when receiving internal and surface PD activities. The sensitivity and reliability of these sensors in the detection of PD faults were proven. Moreover, an outline of the integration of such sensors with an existing SCADA or protection system was given.

### 3.3. VHF/UHF Antennas

The EM-radiated pulse, due to the current through the voids/impurities, propagates from the PD source, containing a combination of different frequency components up to a few GHz, and falling within the range of VHF and UHF bands. The main advantages of the radiometric detection of these PD pulses are to: (i) monitor all apparatus online; (ii) locate the site of partial discharge; and (iii) to some extent, classify the type of PD (need to have the grid frequency as a reference). However, the frequency content of signals from PDs can vary widely depending on (i) the location of the discharge, (ii) the propagation path through the apparatus, (iii) RF interference with power lines and surrounding HV equipment, and (iv) other sources of interference from telecommunications systems such as FM radio, TV broadcast, Wi-Fi, mobile telecommunications, etc., which can affect and reduce the accuracy of the on-site UHF method by passing the signal-included frequencies to tens of kHz and several MHz. Thus, incorrect monitoring information may occur due to such interference. Therefore, it is necessary to use antennas with sufficiently wide passbands (ultra-wideband—UBW) to optimize the measurement. For this reason, broadband antennas are of particular interest in partial discharge classification applications, and maximizing bandwidth while maintaining compactness will be one of the antenna design goals. Log-periodic and fractal schemes can be used to improve the bandwidth, although their size can increase substantially when they are used in the low-frequency range of the UHF band.

As shown in Figure 12, a UHF sensor is important in PD measurement since the first stage in the detection chain is to capture electromagnetic signals for subsequent signal processing utilizing these devices. Consequently, the performance of the sensors will have a significant impact on the accuracy and sensitivity of the PD detection system. UHF sensors might be considered antennas due to the nature of the detected signal, as these sensors are necessary to receive the generated EM waves from the PD source.

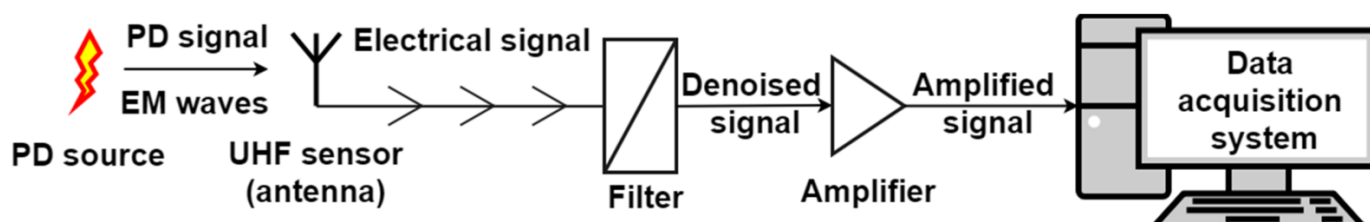


Figure 12. The principal of VHF/UHF detection [22].

Several common VHF/UHF sensors designed for PD detection are introduced thereafter. Figure 12, at the end of this paper, presents a variety of UHF antennas, each with comparable advantages and limitations in terms of operation, structure, and operational characteristics. In an effort to enhance the antenna's performance, various research studies have studied the optimization of antenna parameters through modeling and experimental measurements to obtain a greater level of detection sensitivity and accuracy. With the growing demand for miniaturization, wide bandwidth, and better sensitivity, the UHF

detection mechanism offers a wide detection range, excellent sensitivity, and reduced external disturbances [99].

### 3.3.1. VHF Antennas

In some circumstances, due to attenuation of the UHF components of the PD pulse due to reflection and propagation over long distances, mostly only HF and VHF components remain [100]. However, very high frequency (VHF) sensors are not very common due to their large size and indoor installation, which can be difficult and risky [13]. The VHF method typically entails detecting the VHF signal with an antenna or a window-type sensor mounted directly to the apparatus case. While UHF antennas are typically placed in equipment via oil drain valves or dielectric windows to pick up UHF signals.

Tang et al. [101] established mathematical models to facilitate the theoretical simulation of different isolation defects in GIS. With an the ultra-wideband (UWB) detection in the VHF range, PD signals of four typical faults were detected and acquired using a high-performance stainless steel inner loop sensor in the GIS. Based on the experimental results, the analysis indicated that the VHF PD signals resulting from these different types of defects were similar in the frequency domain but exhibited a large diversity of waveforms in the time and time-frequency domains. Thungsook et al. [102] tested the performance of three different VHF antennas for PD measurements at five test positions, namely 1, 2, 3, 4, and 5 m from the source. Antenna #1 has dimensions of 53 cm in length and 47 mm in width, with a bandwidth of 150 MHz to 1 GHz (Figure 13a); antenna #2 has dimensions of 97 cm by 18 mm; and antenna #3 has dimensions of 178 cm in length and a varying diameter of 1.2 mm to 8 mm. The pulse current transients were detected using a coupling capacitor and an HFCT sensor, while the electromagnetic wave was detected using the VHF antennas. Experimental results showed that the PRPD patterns of VHF PD measurement and HF PD measurement had very similar patterns. In conclusion, the proposed VHF antenna could provide useful information for determining the severity of PD.

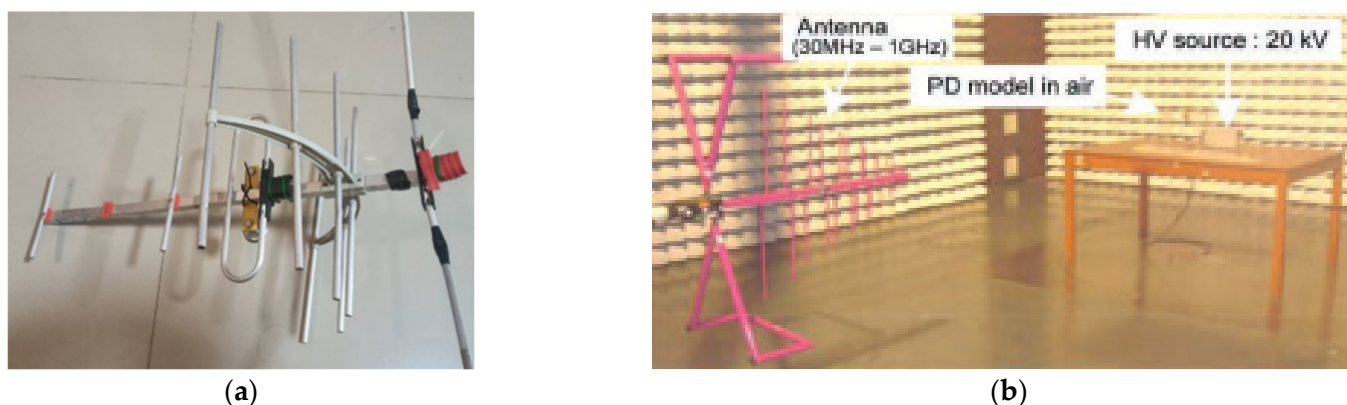


**Figure 13.** The log-periodic antenna for PD measurement: (a) in air with a bandwidth of 150 MHz to 1 GHz [102], and (b) inside oil-paper insulation with a bandwidth of 30 MHz to 1 GHz [103].

Ahmed and Srinivas [72] presented an online PD detection technique using a VHF spectrum analyzer in wire-screened and solidly shielded power cables. The suitability and sensitivity of the VHF method were as good as the two alternative PD detection techniques: HFCT and coupling capacitor. Maneerot et al. [103] compared the performance of a capacitive sensor, used to detect the HF electric field caused by charge transfer inside oil-paper insulation due to PD at the defect site, and a VHF/UHF log-periodic antenna used for detecting electromagnetic PD transients in the air outside the transformer being studied in the near-field region (Figure 13b). The antenna bandwidth was from 30 MHz to 1 GHz. Three types of artificial PD sources in air and in an insulating liquid were investigated. Zhang and Glover [51] presented a compact ultra-wideband printed monopole antenna (PMA) for free-space radiometric PD detection. The antenna had a co-planar waveguide

(CPW) feed and an operating frequency of 120 MHz to 800 MHz, which partially covered the VHF and UHF bands. Due to its low operating frequency, the proposed antenna was quite large, with dimensions of  $70 \times 64$  cm, which limited its practical application in PD detection. As a result, the designed PMA was presented only theoretically, without any practical PD measurement.

### 3.3.2. Wire Antennas

The simplest form of a wire antenna is the monopole antenna, which is a half-dipole antenna mounted above some sort of ground plane (Figure 14a). Monopole antennas are extensively employed in PD detection due to their simple structure, excellent radiation pattern, and appropriate size. However, the operational bandwidth of typical monopole antennas is limited, resulting in information loss [104]. Various UHF wire antennas have been used to detect PD under online conditions in laboratory experiments. Albarracin et al. [105] presented a monopole antenna used in a transformer tank for PD diagnostics. The designed antenna had a size of less than 10 cm (Figure 14b), which was below the diameter of the dielectric windows of the power transformer enclosure (the oil drain valve). The experiment was carried out in both positions inside and outside the transformer tank (Figure 14c). The monopole antenna was used for picking up background noise and PD signal detection. Based on modeling and testing results, the antenna with the smallest size had the maximum sensitivity for PD activities compared to larger antennas. However, based on the SNR, inception voltage, and signal classification rate, it was concluded that the monopole antenna was capable of capturing PD from anywhere near the transformer tank. It was concluded that the PD source and the enclosure resonance modes are the main factors to be considered in PD acquisitions with UHF monopole sensors.

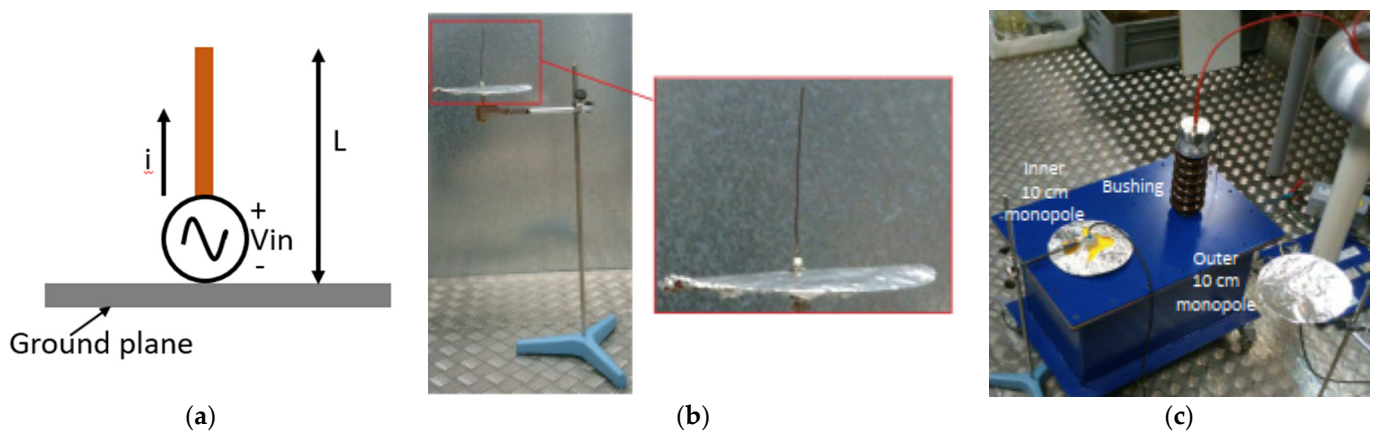


**Figure 14.** The monopole antenna: (a) basic design, (b) the designed monopole antenna with ground plane [105], and (c) two antennas inside and outside the tank to measure surface PD from the bushing insulator [105].

### 3.3.3. PCB Trace Antennas

The main challenge in antenna design is to have a wide frequency bandwidth while keeping a compact size, which is difficult to achieve. Given the frequency spectrum of PDs, UHF antennas naturally need large dimensions for PD detection. As a result, in most common design methods, further miniaturization is often sought. In this regard, some researchers have attempted to miniaturize the UWB UHF antenna by implementing some hybrid design techniques of non-uniform element spacing and combinatorial cyclic different sets, such as fractal antenna design, with appropriate feeding techniques. The antennas are gaining improvements; however, it was not sufficient for UHF operating antenna designs, although some researchers used stacked layer techniques, based on multilayered substrates, and incorporated metamaterial for superstrate antennas, etc., in order to increase

the antenna gain, which is considered one of the most important parameters for early PD signal detection.

(a) *Fractal antennas*

A fractal-based antenna can be described by self-similarity in the repetition of a motif over two or more scale sizes, or iterations, to fill up a given total surface. The objective is to maximize the effective length or increase the material perimeter in order to have exceptional performance in coupling the UHF signal and to provide a broad bandwidth. Several patterns are used in fractal antenna design for PD detection, such as Hilbert, Peano, Moore, Koch, Minkowski, etc. The fractal antenna has various advantages over other types, including its ease of fabrication by etching or photolithography and its ability to be fed via 50-ohm coaxial cable in its bandwidth.

Hilbert's fractal antenna has been introduced by referring to the fractal curve of Hilbert, which is a continuous curve with tight self-similarity for optimal space filling. If the order of the curve increases, the length of the fractal Hilbert curve should increase. Figure 15a shows third- and fourth-order Hilbert fractal antennas. It has been found that a fourth-order Hilbert fractal antenna (Figure 15b) plays the same role as a multiple multi-resonance circuit [106].

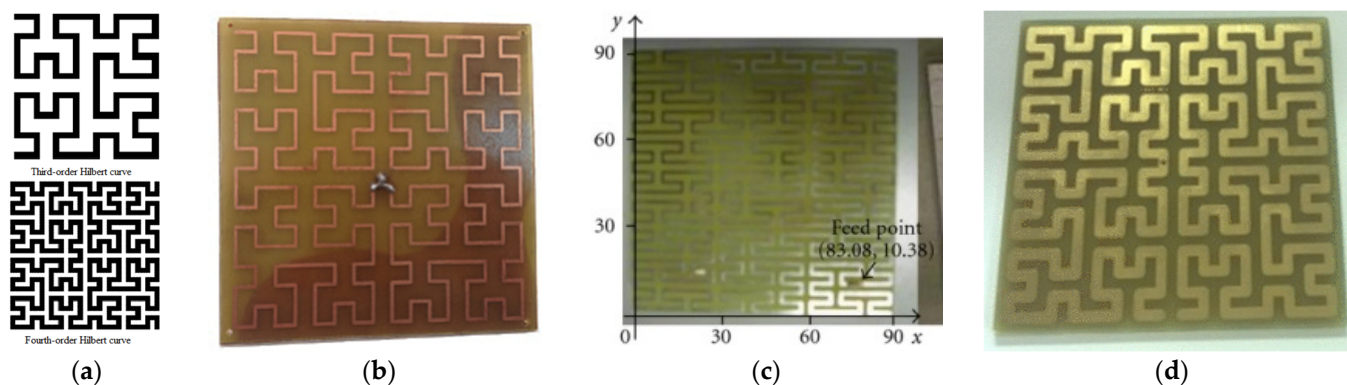


**Figure 15.** Fractal antennas: (a) Third- and fourth-order Hilbert iteration layout, (b) The front face of the fourth-order Hilbert fractal antenna on an FR4 substrate studied in [106], (c) The third-order Peano fractal antenna studied in [107,108], and (d) Moore's fractal antenna studied in [109].

Li et al. [110] presented a small-sized third-order multiband Peano fractal antenna (Figure 15c) for online UHF monitoring of PDs in transformers. Under roughly equivalent dimensions, the first resonant frequency of the Peano fractal antenna was lower than that of the Hilbert. PD experiments were carried out for two artificial insulation defects, corona and surface in oil, in order to compare the proposed antenna and that of the Hilbert. Experimental results showed that the Peano antenna was well qualified for online UHF PD monitoring and was slightly better suited for pattern recognition by analyzing the waveforms of detected PD signals. Wang et al. [109] presented a comparative study between a Moore fractal antenna (Figure 15d) and a Hilbert antenna for PD detection in GISs. Thus, the two antennas were compared in terms of size, multiband, characteristics, performance analysis, radiation, and VSWR. The results showed that both structures could detect the PD signal in the GIS, but with better reception sensitivity for Moore. Indeed, the Moore antenna radiation and VSWR were better and provided a more accurate and faster response to detect PD signals, which showed promise for online PD detection applications.

Li et al. [111] optimized a fourth-order Hilbert fractal antenna for PD measurement to be placed in the dielectric windows of a tank oil-filled transformer. The main objective was to design a compact (20 cm or less) multiband antenna with a high resonance mode. The final structure showed that an operational frequency range of 0.3–1.0 GHz could be achieved with a VSWR of less than 5. The optimum antenna bandwidth was a few hundred MHz. Laboratory tests for two internal defects (superficial and corona discharges) showed

that the antenna detected the PD pulse with an output amplitude voltage of 30.6 mV (equivalent to 33.88 pC of apparent charge) and 47.6 mV (equivalent to 51.36 pC). The results showed that the proposed UHF antenna was qualified for PD online monitoring. Zahed et al. [112] presented a Hilbert fractal antenna for detecting and classifying different types of PDs in an oil-and-paper-insulated system. Three common types of PD were considered: corona, surface, and internal. A recognition rate of 95% was achieved when classifying the different types of PDs. Darmaw and Khayam [113] explored the order effect of Hilbert fractal antennas (second-, third-, and fourth-orders) and the effect of size on PD detection performance. Accordingly, the larger the order, the wider the bandwidth, and the smaller the size, the lower the resonant frequency. Li et al. [110] designed a meandering fractal structure for the online monitoring of PDs in transformers. Experimental results demonstrated that the gain in terms of radiation pattern grew significantly when increasing the antenna order. The proposed meander antenna was tested for two common artificial insulation defects, namely surface discharge in oil and internal discharge in air. The output voltage obtained was around 0.1 V for the surface discharge and 0.2 V for the gas cavity discharge, over a frequency band ranging from 300 MHz to 1 GHz. Experimental results showed that the proposed antenna could be effectively applied for online monitoring and recognition of PD in transformers. Salah et al. [114] discussed the use of an ultra-wide passband 4th-order Hilbert fractal antenna to detect PD in an oil-filled power transformer. The antenna had a multi-operational frequency range of 1.4 to 1.85 GHz, 2.2 to 2.65 GHz, and 3.2 to 3.4 GHz with a VSWR of less than 2. The results showed that the antenna detected PDs with average output voltages of 0.14, 0.12, 1.26, and 1.24 V in different fault configurations (corona in air, sharp edge in oil, surface discharge, and internal void discharge) at a fixed distance of 40 cm from the PD source. Normalized power frequency spectra of captured PD signals from the four faults showed that each type had a different signature, which could help in online discrimination. Wang et al. [115] introduced the Minkowski fractal antenna and revealed that the order of the fractal curve had a substantial impact on the antenna's performance.

(b) *Microstrip antennas*

The PCB-printed type of the monopole antenna, called the microstrip printed monopole antenna (PMA) or patch antenna, has also been suggested for PD detection in the UHF domain [116]. Figure 16 illustrates the basic construction of a microstrip antenna. This technology made great progress in the 1970s and 1980s in the field of communication devices [10]. Patch antennas are primarily used in telecommunications applications and have high gain when matched to a specific resonant frequency. By optimizing the sensor design, greater frequency bandwidth can be achieved for PD detection in a wide UHF range. Due to the key benefits of microstrip antennas, which consist of a tiny thickness, low mass, a cheap manufacturing cost, and a compact volume, this form of sensor might be a viable alternative to commercial UHF probes. However, the fundamental constraints of such an antenna are its limited bandwidth and significant ohmic and dielectric losses.

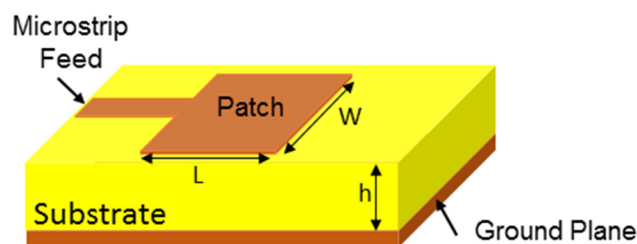
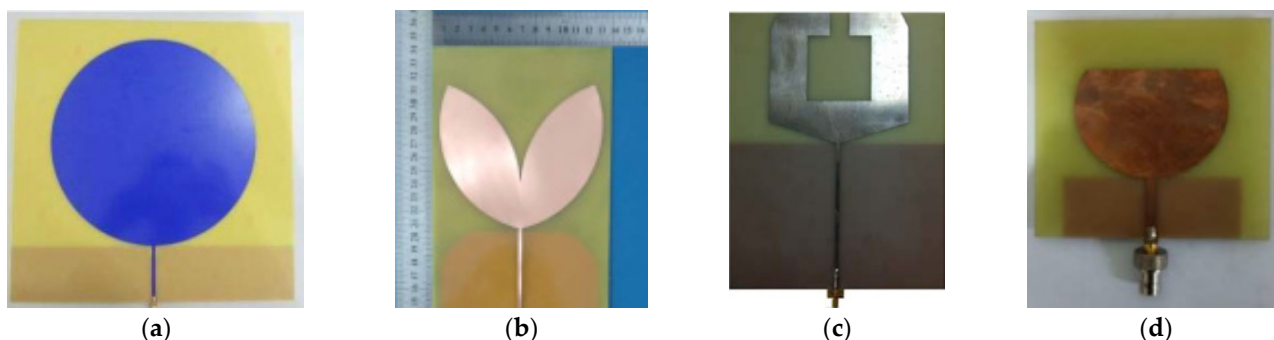


Figure 16. Basic design of the microstrip Antenna.

Sakar et al. [117] discussed the design and performance of a microstrip patch antenna as a UHF sensor. The experimental results showed that the sensors had the ability to detect PD signals below 19 pC, which is proportional to 100 mV, generated by the test setup with

a frequency band ranging from 350 to 800 MHz. In addition, the designed UHF sensor successfully detected PDs at a distance of 6 m. Xavier et al. [118] investigated the utility of a printed monopole antenna with a circular patch for PD detection (Figure 17a). The antenna had a frequency range that covered almost the entire spectrum of PD activity, starting from 312 to 1481 MHz. The final dimensions of the proposed antenna were  $30 \times 30 \text{ cm}^2$ . In laboratory tests, the results showed that the antenna had the ability to detect PD activities with a charge value of 30 pC, indicating high measurement sensitivity. The authors confirmed the detection of PD activity at various frequencies ranging from 333 MHz to 1.21 GHz. Despite the efficiency of the patch antenna, the final dimensions make it more suitable for PD detection when placed in environments with greater flexibility in space, such as in HV equipment surveillance in open power stations. Indeed, additional miniaturization techniques are required for applications in environments with dimensional constraints, such as dielectric windows. Cruz et al. [119] developed a miniaturized printed monopole antenna for PD detection. The latter's geometry was bio-inspired and based on the Inga Marginata leaf (Figure 17b). The antenna had a  $34 \times 14 \text{ cm}^2$  footprint and an operating frequency range from 340 MHz to values above 8 GHz. The results showed that the designed antenna was insensitive to the detection of corona discharges in an open-air power station. Even with its compact dimensions, the bio-inspired antenna was still relatively bulky for applications such as dielectric windows. Thus, according to the authors, the use of this type of sensor in open substations is recommended due to its omnidirectional radiation pattern and its insensitivity to corona discharges. Yang et al. [120] proposed an UWB-printed antenna used for external PD detection in GIS, adopting a modified U-shaped radiating patch similar to [121] (Figure 17c). The results showed that the designed UWB antenna had a bandwidth covering 0.5 to 1.5 GHz, which satisfied the bandwidth criteria for UHF antennas. The latter was tested twice for PD measurements: in the laboratory using an artificial air cavity at a distance of 50 cm and on-site using air-insulated switchgear at a distance of 75 cm. Both tests produced notable results for PD signals. The antenna's average gain and physical size showed that its performance was outstanding when used as an external sensor but may not meet the needs of internal sensors for GIS or transformers. Since this type of antenna can detect a wide variety of frequency components, PD identification can be used with greater accuracy when combined with frequency spectrum analysis. Uwiringiyimana et al. [122] proposed a circular-shaped microstrip patch antenna developed for PD measurement with reduced noise level (Figure 17d). The antenna measured  $100 \times 100 \text{ mm}^2$  and had a bandwidth of 1.2 to 4.5 GHz. The latter was compared to an HFCT for PD tests. At a distance of 70 cm from the source, the UHF antenna detected a peak-to-peak signal of 288 mV for an applied voltage of 7 kV. Telecom background noise was reduced. However, the antenna bandwidth included all other telecommunication bands while excluding only the GSM-900 MHz band. For this reason, noise cancellation was not entirely successful.



**Figure 17.** Microstrip antennas: (a) the circularly printed monopole antenna studied in [118], (b) the bio-inspired antenna based on the Inga Marginata studied in [119], (c) the UWB-printed antenna with a modified U-shaped proposed and studied in [120], and (d) the circular-shaped microstrip patch antenna studied in [122].

(c) *Spiral antennas*

Spiral antennas have the shape of a two-armed spiral fed by a coplanar waveguide line [123]. The Archimedean spiral antenna (Figure 18a) is a type of spiral antenna. It has attracted much interest as UHF sensors for PD diagnostics due to their polarization-independent radiation pattern. Lozano-Claros et al. [123] examined two different types of antennas, namely a planar complex spiral antenna and a fractal tree log-periodic dipole antenna, both located on the GIS junction of two segments. The spiral antenna has a bandwidth of 300 to 700 MHz, while the dipole antenna has a bandwidth of 700 MHz to 1.5 GHz. The spiral antenna has a diameter of 19.1 cm and is made on a 2.5 mm-thick substrate. The spiral antenna was difficult to design despite its wide bandwidth, which covers the entire spectrum of PD activity. Indeed, it was difficult to determine the ideal number of turns in order to combine between the two antennas, and the assembly of the two structures required a complex design process (Figure 18b). It was found that antenna miniaturization can be achieved by using substrate permittivity greater than 10.7, but at the cost of lower antenna gain performance. This paper successfully confirmed that the planar complex spiral antenna is suitable for PD detection in GIS.

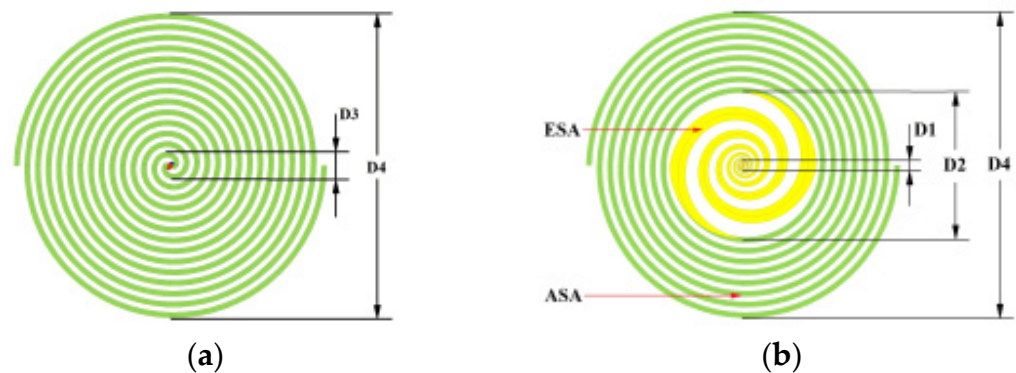


**Figure 18.** The (a) Archimedean spiral antenna, and (b) Planar complex spiral antenna proposed in [123].

Park and Jung [124] proposed an Archimedean spiral antenna for PD detection operating in the frequency range of 0.6 to 1.7 GHz (Figure 19a). The antenna structure had a diameter of 190 mm and a height of 153 mm. The fabricated antenna had the potential to be used in PD detection because its reflection coefficient, radiation pattern, and gain values were very similar to the simulations. The approach had not been tested for real-world online PD measurement, however. Yadam et al. [125] proposed a cosine-slot cavity-backed Archimedean spiral antenna (CSAS) for PD diagnostics (Figure 19b). The dual-arm slotted spiral has been meandered like a cosine wave for size reduction and optimized for broadband operation with circular polarization (CP) on 0.5–5 GHz. The sensor featured a wide bandwidth beyond the UHF range, up to 4 GHz. Additionally, the average gain in the range where PD occurred most frequently was well below 2 dBi. The results showed that the designed CSAS was able to detect and classify three types of PD defects, namely particle movement, corona, and surface discharge, due to its consistent circular polarization. It is well known that spiral antennas have difficult profiles for integration since they occupy a large area. Therefore, they are not advised in cases where there are small spaces for PD detection in electrical equipment. Li et al. [126] designed and optimized a two-arm equiangular spiral antenna for PD detection. Simulation and test results showed good agreement and verified that the designed sensors could well meet the GIS internal partial discharge monitoring requirements in terms of bandwidth, performance, size, etc.



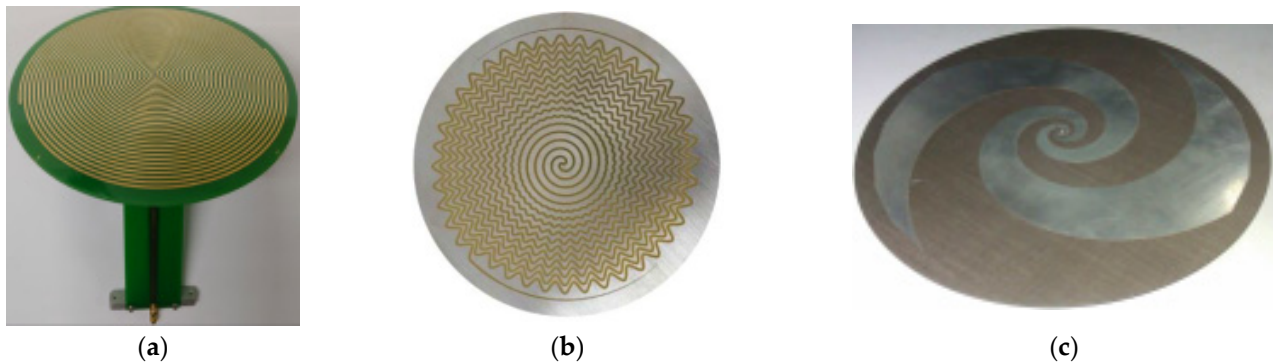


**Figure 19.** Different designs of spiral antennas: (a) the Archimedean spiral antenna studied in [124], (b) the cavity-backed cosine slot Archimedean spiral antenna studied in [125], and (c) the two-arm equiangular spiral antenna studied in [126].

Archimedean spiral antennas have recently been printed on flexible substrates so that they can be easily bent or attached to the body of the equipment. Cheng et al. [127] designed and miniaturized a UHF Archimedean spiral antenna based on a flexible thermosetting polyimide (TPI) substrate for PD detection (Figure 20). The flexible antenna had a diameter of 149 mm, which was 24.7% less than the non-miniaturized antenna. The VSWR of the flexible antenna was  $\leq 2$  at a bend radius of 0, 250, 300, and 350 mm in the 610 MHz to 3 GHz band, and the maximum gain was 5.5 dB, with excellent radiation performance. The performances in PD detection were measured, and the results showed that the latter could effectively detect the PD signal before and after the bending deformation. Undoubtedly, printable UHF antennas on flexible-based substrates represent research for the future.

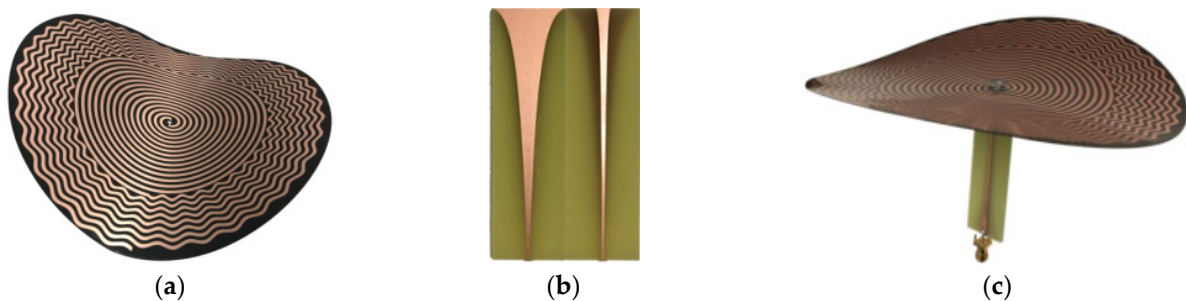


**Figure 20.** The flexible Archimedes spiral antenna studied in [127]: (a) the antenna body on a flexible thermosetting polyimide (TPI) substrate, (b) the antenna feedline, which is an exponential gradient microstrip balun, and (c) the total assembled structure.

#### (d) Biconical antennas

Bowtie antennas, a subfamily of biconical antennas, are another popular option for PD detection in the UHF range [128,129]. These antennas are simple to manufacture using printable technology because of their bow tie design. Daulay and Khayam [130] proposed a series of dual-layer bowtie antennas with edge and middle sliced modifications for detecting PDs (Figure 21a). The antenna, which measured  $160 \times 54 \text{ mm}^2$  and was built on a 1.6 mm-thick FR4 board, had a return loss of 10 dB and a VSWR of 2. Real-world PD tests were not performed. Uwiringiyimana and Khayam [131] designed a double-layer bowtie antenna by modifying the wings' shape (Figure 21b) for corona PD measurement. The bowtie antenna was tested and compared with a conventional RC detector. Since the antenna's bandwidth included several communication bands as background noise while excluding the region where PD occurs most frequently, the antenna's ability to detect PD signals was limited.



**Figure 21.** (a) A series of double-layer bowtie antennas with edge and middle sliced modifications a top view studied in [130], and (b) The double-layer bowtie antenna studied in [129].

### (e) Aperture Antennas

Vivaldi antennas, a subfamily of aperture antennas, are common for PD detection. This type of antenna is composed of two copper parts, one of which is separated from the other by a dielectric substrate. This antenna consists of a slot line that is embedded in a dielectric substrate. Vivaldi antennas are considered non-resonant, and by improving the slot and feeding shapes, a wide bandwidth can be achieved. If an EM signal's wavelength is greater than the maximum slot width of the Vivaldi antenna, the latter cannot radiate effectively [132]. Depending on the feeding mode, there are three types of Vivaldi antennas: antipodal, normal, and balanced. Vivaldi antennas can detect EM pulses with a low-frequency component generated from corona and surface PDs, although they are designed for high frequencies. Therefore, these antennas are susceptible to interference with FM radio and low-frequency television broadcasts. Zhang et al. [132] suggested an antipodal Vivaldi antenna (Figure 22a). The latter, which was designed on a Teflon substrate instead of the more common FR4 substrate, makes a justifiable argument by claiming that FR-4 struggles to keep the doping concentrations of different manufacturers under control. The FR-4 substrate had good performance below 1 GHz, but due to its high dielectric loss above this frequency, the antenna gain became low, which is undesirable for early PD detection. Saleh et al. [133] proposed a compact UWB Vivaldi conical slot antenna (Figure 22b).

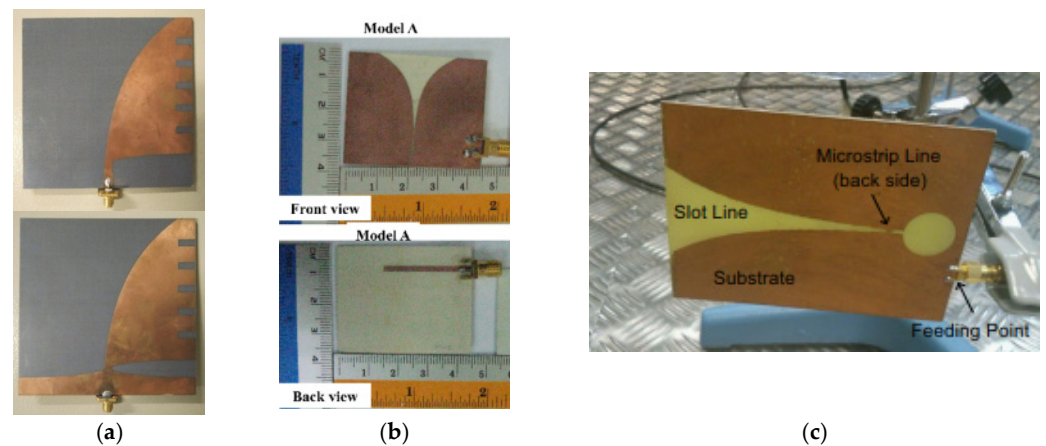


**Figure 22.** Aperture antennas: (a) antipodal Vivaldi antenna used in [132], (b) compact UWB Vivaldi tapered slot antenna [133], and (c) Vivaldi antenna studied in [134].

Albarracin et al. [134] proposed a Vivaldi antenna with a bandwidth ranging from 1.3 to 3.0 GHz (Figure 22c). Although this also contained communication noises, the antenna was not naturally able to separate. Results showed that at a distance of 1 m and by turning on only the Wi-Fi signals, PD pulses were detected in a noisy environment. As has already been noted, antennae with bowtie, spiral, and Vivaldi shape designs typically experience complicated construction, particularly because they require sophisticated balun-based feeding methods. In order to diagnose PD, Vivaldi antennas face integration challenges with electrical equipment.

Table 2 summarizes all the UHF antennas used for PD detection described in the paper, along with their performance.

**Table 2.** Comparison between UHF sensor designs proposed for PD detection.

Antenna Type	Pattern Type	Physical Size	VSWR	Bandwidth	Application Test	Ref.
Fractal antennas	Hilbert	110 mm	<2	0.8–2 GHz	PD model	[106]
	Peano	90 mm	<5	0.3–1 GHz	PD model	[107,108]
	Moore	65 mm	<2	0.3–3 GHz	GIS	[109]
	Hilbert	100 mm	<5	0.3–1 GHz	Transformer	[111]
	Hilbert	100 mm	-	0.1–3 GHz	PD model	[112]
	Hilbert	105 mm	-	0.3–3 GHz	-	[113]
	Meander	70 mm	<2	0.3–1 GHz	Transformer	[110]
	Hilbert	80 mm	<2	0.3–4 GHz	PD model	[114]
	Minkowski	300 mm	-	0.7–3 GHz	Transformer	[115]
	Hilbert	100 mm	-	0.3–3 GHz	PD model	[135]
Microstrip antennas	Monopole	100 mm	-	0.5–2.5 GHz	Transformer	[105]
	Squared	232 mm	-	0.35–0.8 GHz	High-voltage equipment	[117]
	Circular	320 mm	-	0.3–1.5 GHz	PD model	[118]
	U-shaped	215 mm	-	0.5–1.5 GHz	High-voltage switchgears	[120]
	Microstrip	105 mm	<2	0.5–1.5 GHz	-	[121]
	Microstrip patch	100 mm	<2	1.2–4.5 GHz	PD model	[122]
	Microstrip patch	100 mm	<2	1.18–3 GHz	Transformer	[136]
	Conical	100 mm	<5	0.6–3 GHz	Transformer	[137]
	Circular	100 mm	<2	1.2–3 GHz	Transformer	[138]
	Koch Snowflake	280 mm	<5	0.3–1 GHz	High-voltage switchgears	[139]
Spiral antennas	planar complex	191 mm	$\leq 2$	0.3–3 GHz	GIS	[123]
	Archimedean	190 mm	-	0.6–1.7 GHz	-	[124]
	cavity-backed cosine slot	70 mm	-	0.5–5 GHz	PD model	[125]
	Two Arm equiangular	150 mm	-	0.7–3 GHz	GIS	[126]
	Archimedean	198 mm	$\leq 2$	0.61–3 GHz	High-voltage switchgears	[127]
	Single Arm	200 mm	-	1.15–2.4 GHz	Transformer	[140]
Biconical antennas	Asymmetric biconical	150 mm/ 95 mm	<2	0.47–3 GHz	Power substation	[46]
	Long bowtie	60 mm	$\leq 2$	0.8–1.06 GHz/ 2.01–2.63 GHz	GIS	[128]
	Bowtie	100 mm	<2	782 MHz	GIS	[129]
	Double layer bowtie	36 mm	<2	1.576–2.1 GHz	PD model	[131]
Aperture antennas	Antipodal Vivaldi	100 mm	-	0.8–3 GHz	Transformer	[132]
	Tapered Slot	270 mm	-	3.1–10.6 GHz	-	[133]
	Vivaldi	120 mm	-	1.3–3 GHz	PD model	[134]

#### 4. Conclusions

High-voltage system designers and maintenance engineers have not and will never disregard the challenges connected with PD for high-voltage equipment and high-voltage power systems. In cases of high voltage, PD detection and monitoring make economic sense in the short and long terms. What sensors to use, how reliable they are, and how quickly they can monitor PD have all become hot topics. This study has gone to great efforts to present a detailed review of PD detection by means of radiated high-frequency electromagnetic fields. In this overview, several types of radio-frequency sensors have been exhaustively described in terms of their principles of function and performance. Hence, a new generic categorization approach based on the detected electromagnetic wave component (B-field or E-field) and pick-up location, either from free space or ground cable, is introduced. Accordingly, radio-frequency (RF) sensors are divided into three categories: inductive sensors, loop antennas, and VHF/UHF antennas. A loop antenna couples the magnetic field generated by the PD signal, while the VHF/UHF antenna measures the high-frequency components of the electric field. The operating principle and the different techniques deployed in each category have been detailed in the paper.

**Author Contributions:** Conceptualization, M.H.S. and B.M.; methodology, S.K., M.H.S. and F.T.; validation, S.K., A.I. and B.M.; formal analysis, S.K. and M.H.S.; investigation, F.T. and D.F.; writing—original draft preparation, S.K., M.H.S. and A.I.; writing—review and editing, S.K., F.T. and D.F.; visualization, F.T., P.R. and D.F.; supervision, D.F., P.R. and F.T.; project administration, D.F.; funding acquisition, D.F. All authors have read and agreed to the published version of the manuscript.

**Funding:** This work was carried out with the support of a Marie Skłodowska-Curie individual fellowship, project reference 101030887.

**Data Availability Statement:** Data is contained within the article.

**Conflicts of Interest:** The authors declare no conflict of interest.

#### References

1. Liao, Y.; Liu, H.; Yuan, J.; Xu, Y.; Zhou, W.; Zhou, C. A holistic approach to risk-based maintenance scheduling for HV cables. *IEEE Access* **2019**, *7*, 118975–118985. [[CrossRef](#)]
2. Montanari, G.C.; Mazzanti, G. Ageing of polymeric insulating materials and insulation system design. *Polym. Int.* **2002**, *51*, 1151–1158. [[CrossRef](#)]
3. Afia, R.S.; Mustafa, E.; Tamus, Z.Á. Aging Assessment of XLPE/CSPE LV Nuclear Power Cables Under Simultaneous Radiation-Mechanical Stresses. *Energy Rep.* **2022**, *8*, 1028–1037. [[CrossRef](#)]
4. Gjerde, A. Multifactor ageing models—origin and similarities. *IEEE Electr. Insul. Mag.* **1997**, *13*, 6–13. [[CrossRef](#)]
5. Morshuis, P.H.F. Partial Discharge Mechanisms: Mechanisms Leading to Breakdown, Analyzed by Fast Electrical and Optical Measurements. Ph.D. Thesis, Delft University of Technology, Delft, The Netherlands, 1993.
6. Ardila-Rey, J.A.; Cerda-Luna, M.P.; Rozas-Valderrama, R.A.; De Castro, B.A.; Andreoli, A.L.; Muhammad-Sukki, F. Separation techniques of partial discharges and electrical noise sources: A review of recent progress. *IEEE Access* **2020**, *8*, 199449–199461. [[CrossRef](#)]
7. Morshuis, P.H. Degradation of solid dielectrics due to internal partial discharge: Some thoughts on progress made and where to go now. *IEEE Trans. Dielectr. Electr. Insul.* **2005**, *12*, 905–913. [[CrossRef](#)]
8. Niemeyer, L. A generalized approach to partial discharge modeling. *IEEE Trans. Dielectr. Electr. Insul.* **1995**, *2*, 510–528. [[CrossRef](#)]
9. Moradnouri, A.; Vakilian, M.; Hekmati, A.; Fardmanesh, M. HTS transformer's partial discharges raised by floating particles and nitrogen bubbles. *J. Supercond. Nov. Magn.* **2020**, *33*, 3027–3034. [[CrossRef](#)]
10. Kreuger, F.; Gulski, E.; Krivda, A. Classification of partial discharges. *IEEE Trans. Electr. Insul.* **1993**, *28*, 917–931. [[CrossRef](#)]
11. Cavallini, A.; Montanari, G.; Puletti, F.; Contin, A. A new methodology for the identification of PD in electrical apparatus: Properties and applications. *IEEE Trans. Dielectr. Electr. Insul.* **2005**, *12*, 203–215. [[CrossRef](#)]
12. Wu, M.; Cao, H.; Cao, J.; Nguyen, H.-L.; Gomes, J.B.; Krishnaswamy, S.P. An overview of state-of-the-art partial discharge analysis techniques for condition monitoring. *IEEE Electr. Insul. Mag.* **2015**, *31*, 22–35. [[CrossRef](#)]
13. Lu, S.; Chai, H.; Sahoo, A.; Phung, B. Condition monitoring based on partial discharge diagnostics using machine learning methods: A comprehensive state-of-the-art review. *IEEE Trans. Dielectr. Electr. Insul.* **2020**, *27*, 1861–1888. [[CrossRef](#)]
14. Biswas, S.; Koley, C.; Chatterjee, B.; Chakravorti, S. A methodology for identification and localization of partial discharge sources using optical sensors. *IEEE Trans. Dielectr. Electr. Insul.* **2012**, *19*, 18–28. [[CrossRef](#)]
15. Duval, M. A review of faults detectable by gas-in-oil analysis in transformers. *IEEE Electr. Insul. Mag.* **2002**, *18*, 8–17. [[CrossRef](#)]

16. Descoeudres, A.; Hollenstein, C.; Demellayer, R.; Walder, G. Optical emission spectroscopy of electrical discharge machining plasma. *J. Phys. D Appl. Phys.* **2004**, *37*, 875. [[CrossRef](#)]
17. Ilkhechi, H.D.; Samimi, M.H. Applications of the acoustic method in partial discharge measurement: A review. *IEEE Trans. Dielectr. Electr. Insul.* **2021**, *28*, 42–51. [[CrossRef](#)]
18. Morsalin, S.; Das, N. Diagnostic aspects of partial discharge measurement at very low frequency: A review. *IET Sci. Meas. Technol.* **2020**, *14*, 825–841. [[CrossRef](#)]
19. Rostamina, R.; Saniei, M.; Vakilian, M.; Mortazavi, S.S. Evaluation of transformer core contribution to partial discharge electromagnetic waves propagation. *Int. J. Electr. Power Energy Syst.* **2016**, *83*, 40–48. [[CrossRef](#)]
20. Upton, D.W.; Mistry, K.K.; Mather, P.J.; Zaharis, Z.D.; Atkinson, R.C.; Tachtatzis, C.; Lazaridis, P.I. A review of techniques for RSS-based radiometric partial discharge localization. *Sensors* **2021**, *21*, 909. [[CrossRef](#)]
21. Samimi, M.H.; Mahari, A.; Farahnakian, M.A.; Mohseni, H. The Rogowski coil principles and applications: A review. *IEEE Sens. J.* **2014**, *15*, 651–658. [[CrossRef](#)]
22. Chai, H.; Phung, B.T.; Mitchell, S. Application of UHF sensors in power system equipment for partial discharge detection: A review. *Sensors* **2019**, *19*, 1029. [[CrossRef](#)] [[PubMed](#)]
23. Roslizan, N.; Rohani, M.; Wooi, C.; Isa, M.; Ismail, B.; Rosmi, A.; Mustafa, W. A review: Partial discharge detection using UHF sensor on high voltage equipment. *J. Phys. Conf. Ser.* **2020**, *1432*, 012003. [[CrossRef](#)]
24. Hikita, M.; Ohtsuka, S.; Matsumoto, S. Recent trend of the partial discharge measurement technique using the UHF electromagnetic wave detection method. *IEEJ Trans. Electr. Electron. Eng.* **2007**, *2*, 504–509. [[CrossRef](#)]
25. Tenbohlen, S.; Beura, C.P.; Sikorski, W.; Sanchez, R.A.; de Castro, B.A.; Beltle, M.; Fehlmann, P.; Judd, M.; Werner, F.; Siegel, M. Frequency Range of UHF PD Measurements in Power Transformers. *Energies* **2023**, *16*, 1395. [[CrossRef](#)]
26. Mondal, M.; Kumbhar, G.B. Detection, measurement, and classification of partial discharge in a power transformer: Methods, trends, and future research. *IETE Tech. Rev.* **2018**, *35*, 483–493. [[CrossRef](#)]
27. Mondal, M.; Kumbhar, G.B. Partial discharge localization in a power transformer: Methods, trends, and future research. *IETE Tech. Rev.* **2017**, *34*, 504–513. [[CrossRef](#)]
28. Bartnikas, R. Detection of partial discharges (corona) in electrical apparatus. *IEEE Trans. Electr. Insul.* **1990**, *25*, 111–124. [[CrossRef](#)]
29. Bartnikas, R. Partial discharges. Their mechanism, detection and measurement. *IEEE Trans. Dielectr. Electr. Insul.* **2002**, *9*, 763–808. [[CrossRef](#)]
30. Pan, C.; Wu, K.; Chen, G.; Gao, Y.; Florkowski, M.; Lv, Z.; Tang, J. Understanding partial discharge behavior from the memory effect induced by residual charges: A review. *IEEE Trans. Dielectr. Electr. Insul.* **2020**, *27*, 1951–1965. [[CrossRef](#)]
31. Van Brunt, R.J.; Cernyar, E.; Von Glahn, P. Importance of unraveling memory propagation effects in interpreting data on partial discharge statistics. *IEEE Trans. Electr. Insul.* **1993**, *28*, 905–916. [[CrossRef](#)]
32. Dissado, L.A. Understanding electrical trees in solids: From experiment to theory. *IEEE Trans. Dielectr. Electr. Insul.* **2002**, *9*, 483–497. [[CrossRef](#)]
33. Stone, G.; Boulter, E.A.; Culbert, I.; Dhirani, H. *Electrical Insulation for Rotating Machines: Design, Evaluation, Aging, Testing, and Repair*; Wiley-IEEE Press: Hoboken, NJ, USA, 2004.
34. Kreuger, F.H. Detection and Location of Discharges. Ph.D. Thesis, Technische Universiteit Delft, Delft, The Nederland, 1961.
35. Gulski, E. Computer-Aided Recognition of Partial Discharges Using Statistical Tools. Ph.D. Thesis, Delft University Press, Delft, The Netherlands, 1991.
36. Contin, A.; Montanari, G.; Ferraro, C. PD source recognition by Weibull processing of pulse height distributions. *IEEE Trans. Dielectr. Electr. Insul.* **2000**, *7*, 48–58. [[CrossRef](#)]
37. Basharan, V.; Siluvairaj, W.I.M.; Velayutham, M.R. Recognition of multiple partial discharge patterns by multi-class support vector machine using fractal image processing technique. *IET Sci. Meas. Technol.* **2018**, *12*, 1031–1038. [[CrossRef](#)]
38. Sahoo, N.; Salama, M.; Bartnikas, R. Trends in partial discharge pattern classification: A survey. *IEEE Trans. Dielectr. Electr. Insul.* **2005**, *12*, 248–264. [[CrossRef](#)]
39. Romano, P.; Imburgia, A.; Ala, G. Partial discharge detection using a spherical electromagnetic sensor. *Sensors* **2019**, *19*, 1014. [[CrossRef](#)]
40. Peng, X.; Yang, F.; Wang, G.; Wu, Y.; Li, L.; Li, Z.; Bhatti, A.A.; Zhou, C.; Hepburn, D.M.; Reid, A.J.; et al. A Convolutional Neural Network-Based Deep Learning Methodology for Recognition of Partial Discharge Patterns from High-Voltage Cables. *IEEE Trans. Power Deliv.* **2019**, *34*, 1460–1469. [[CrossRef](#)]
41. Barrios, S.; Buldain, D.; Comech, M.P.; Gilbert, I.; Orue, I. Partial discharge classification using deep learning methods—Survey of recent progress. *Energies* **2019**, *12*, 2485. [[CrossRef](#)]
42. Cavallini, A.; Montanari, G.; Contin, A.; Pulletti, F. A new approach to the diagnosis of solid insulation systems based on PD signal inference. *IEEE Electr. Insul. Mag.* **2003**, *19*, 23–30. [[CrossRef](#)]
43. Hirata, A.; Nakata, S.; Kawasaki, Z.-I. Toward automatic classification of partial discharge sources with neural networks. *IEEE Trans. Power Deliv.* **2005**, *21*, 526–527. [[CrossRef](#)]
44. Gulski, E.; Krivda, A. Neural networks as a tool for recognition of partial discharges. *IEEE Trans. Electr. Insul.* **1993**, *28*, 984–1001. [[CrossRef](#)]
45. IEEE. *Guide for Partial Discharge Testing of Shielded Power Cable Systems in a Field Environment*; IEEE: New York, NY, USA, 2007.

46. Hu, Y.; Zeng, Z.; Liu, J.; Wang, J.; Zhang, W. Design of a distributed UHF sensor array system for PD detection and location in substation. *IEEE Trans. Instrum. Meas.* **2019**, *68*, 1844–1851. [\[CrossRef\]](#)
47. IEC-60270; High-Voltage Test Techniques: Partial Discharge Measurements. IEC: Geneva, Switzerland, 2000; pp. 13–31.
48. Cheng, C.; Fan, C.-L.; Hsiao, H.-C.; Wang, W.-M. On-site partial discharge measurement of underground cable system. In Proceedings of the 2011 7th Asia-Pacific International Conference on Lightning, Chengdu, China, 1–4 November 2011; pp. 575–580.
49. Bakar, N.A.; Abu-Siada, A.; Islam, S. A review of dissolved gas analysis measurement and interpretation techniques. *IEEE Electr. Insul. Mag.* **2014**, *30*, 39–49. [\[CrossRef\]](#)
50. Danouj, B.; Tahan, S.; David, E. Using a new generation of piezoelectric sensors for partial discharge detection. *Measurement* **2013**, *46*, 660–666. [\[CrossRef\]](#)
51. Zhang, Y.; Glover, I. Design of an ultrawideband VHF/UHF antenna for partial discharge detection. In Proceedings of the 2014 IEEE International Conference on Signal Processing, Communications and Computing (ICSPCC), Guilin, China, 5–8 August 2014; pp. 487–490.
52. Mor, A.R.; Heredia, L.C.C.; Muñoz, F.A. A novel approach for partial discharge measurements on GIS using HFCT sensors. *Sensors* **2018**, *18*, 4482.
53. Kaziz, S.; Imburgia, A.; Flandre, D.; Rizzo, G.; Romano, P.; Viola, F.; Ala, G.; Tounsi, F. Performances of a PCB-based Loop Antenna Inductive Sensor for Partial Discharges Detection. In Proceedings of the 2022 IEEE 4th International Conference on Dielectrics (ICD), Palermo, Italy, 3–7 July 2022; pp. 9–12.
54. Wang, X.; Li, B.; Xiao, Z.; Lee, S.H.; Roman, H.; Russo, O.L.; Chin, K.K.; Farmer, K.R. An ultra-sensitive optical MEMS sensor for partial discharge detection. *J. Micromechan. Microeng.* **2004**, *15*, 521. [\[CrossRef\]](#)
55. Salustiano, R.; Capellini, R.; De Abreu, S.; Martinez, M.; Tavares, I.; Ferraz, G.; Romano, M. Development of new methodology for insulators inspections on aerial distribution lines based on partial discharge detection tools. In Proceedings of the 2014 ICHVE International Conference on High Voltage Engineering and Application, Poznan, Poland, 8–11 September 2014; pp. 1–4.
56. Kanegami, M.; Miyazaki, S.; Miyake, K. Partial Discharge Detection with High-Frequency Band through Resistance-Temperature Sensor of Hydropower Generator Stator Windings. *Electr. Eng. Jpn.* **2016**, *195*, 9–15. [\[CrossRef\]](#)
57. Kindl, V.; Skala, B.; Pechanek, R.; Kus, V.; Hornak, J. Low-pass filter for HV partial discharge testing. *Sensors* **2018**, *18*, 482. [\[CrossRef\]](#) [\[PubMed\]](#)
58. Kaziz, S.; Romano, P.; Imburgia, A.; Ala, G.; Sghaier, H.; Flandre, D.; Tounsi, F. PCB-Based Planar Inductive Loops for Partial Discharges Detection in Power Cables. *Sensors* **2023**, *23*, 290. [\[CrossRef\]](#)
59. Robles, G.; Martinez-Tarifa, J.M.; Rojas-Moreno, M.V.; Sanz-Feito, J. Inductive sensor for measuring high frequency partial discharges within electrical insulation. *IEEE Trans. Instrum. Meas.* **2009**, *58*, 3907–3913. [\[CrossRef\]](#)
60. Rozi, F.; Khayam, U. Development of loop antennas for partial discharge detection. *Int. J. Electr. Eng. Inform.* **2015**, *7*, 29. [\[CrossRef\]](#)
61. Azam, S.K.; Othman, M.; Ilias, H.A.; Latef, T.A.; Islam, M.T.; Ain, M.F. Ultra-high frequency printable antennas for partial discharge diagnostics in high voltage equipment. *Alex. Eng. J.* **2023**, *64*, 709–729. [\[CrossRef\]](#)
62. Schwarz, R.; Muhr, M. Modern technologies in optical partial discharge detection. In Proceedings of the 2007 Annual Report-Conference on Electrical Insulation and Dielectric Phenomena, Vancouver, BC, Canada, 14–17 October 2007; pp. 163–166.
63. Wang, Z.; Cotton, I. Northcote, and others, Dissolved gas analysis of alternative fluids for power transformers. *IEEE Electr. Insul. Mag.* **2007**, *23*, 5–14.
64. Qian, S.; Chen, H.; Xu, Y.; Su, L. High sensitivity detection of partial discharge acoustic emission within power transformer by sagnac fiber optic sensor. *IEEE Trans. Dielectr. Electr. Insul.* **2018**, *25*, 2313–2320. [\[CrossRef\]](#)
65. Chelmiah, E.T.; Kavanagh, D.F. Acoustic Sensor Array Topologies for Partial Discharge Localisation in Electric Machines. In Proceedings of the 2022 International Conference on Electrical Machines (ICEM), Valencia, Spain, 5–8 September 2022; pp. 1582–1588.
66. BúaNúñez, I.; Posada-Román, J.E.; Rubio-Serrano, J.; Garcia-Souto, J.A. Instrumentation system for location of partial discharges using acoustic detection with piezoelectric transducers and optical fiber sensors. *IEEE Trans. Instrum. Meas.* **2013**, *63*, 1002–1013. [\[CrossRef\]](#)
67. Liu, B.; Ma, H.; Ju, P. Partial discharge diagnosis by simultaneous observation of discharge pulses and vibration signal. *IEEE Trans. Dielectr. Electr. Insul.* **2017**, *24*, 288–295. [\[CrossRef\]](#)
68. Posada-Roman, J.; Garcia-Souto, J.A.; Rubio-Serrano, J. Fiber optic sensor for acoustic detection of partial discharges in oil-paper insulated electrical systems. *Sensors* **2012**, *12*, 4793–4802. [\[CrossRef\]](#)
69. Zhou, H.-Y.; Ma, G.-M.; Zhang, M.; Zhang, H.-C.; Li, C.-R. A high sensitivity optical fiber interferometer sensor for acoustic emission detection of partial discharge in power transformer. *IEEE Sens. J.* **2019**, *21*, 24–32. [\[CrossRef\]](#)
70. Campbell, S.; Stone, G. Investigations into the use of temperature detectors as stator winding partial discharge detectors. In Proceedings of the Conference Record of the 2006 IEEE International Symposium on Electrical Insulation, Toronto, ON, Canada, 11–14 June 2006; pp. 369–375.
71. Hampton, B.; Meats, R. Diagnostic measurements at UHF in gas insulated substations. *IEE Proc. C Gener. Transm. Distrib.* **1988**, *135*, 137–144. [\[CrossRef\]](#)
72. Ahmed, N.; Srinivas, N. On-line partial discharge detection in cables. *IEEE Trans. Dielectr. Electr. Insul.* **1998**, *5*, 181–188. [\[CrossRef\]](#)

73. Fritsch, M.; Wolter, M. High-Frequency Current Transformer Design and Construction Guide. *IEEE Trans. Instrum. Meas.* **2022**, *71*, 1–9. [[CrossRef](#)]
74. Zachariades, C.; Shuttleworth, R.; Giussani, R.; MacKinlay, R. Optimization of a high-frequency current transformer sensor for partial discharge detection using finite-element analysis. *IEEE Sens. J.* **2016**, *16*, 7526–7533. [[CrossRef](#)]
75. Álvarez, F.; Garnacho, F.; Ortego, J.; Sánchez-Urán, M.Á. Application of HFCT and UHF sensors in on-line partial discharge measurements for insulation diagnosis of high voltage equipment. *Sensors* **2015**, *15*, 7360–7387. [[CrossRef](#)] [[PubMed](#)]
76. Luo, G.; Zhang, D. Study on performance of HFCT and UHF sensors in partial discharge detection. In Proceedings of the 2010 Conference Proceedings IPEC, Singapore, 27–29 October 2010; pp. 630–635.
77. Paulus, S.; Kammerer, J.-B.; Pascal, J.; Bona, C.; Hebrard, L. Continuous calibration of Rogowski coil current transducer. *Analog. Integr. Circuits Signal Process.* **2016**, *89*, 77–88. [[CrossRef](#)]
78. Hashmi, G.M.; Lehtonen, M.; Nordman, M. Modeling and experimental verification of on-line PD detection in MV covered-conductor overhead networks. *IEEE Trans. Dielectr. Electr. Insul.* **2010**, *17*, 167–180. [[CrossRef](#)]
79. Moreno, M.V.R.; Robles, G.; Albarracin, R.; Rey, J.A.; Tarifa, J.M.M. Study on the self-integration of a Rogowski coil used in the measurement of partial discharges pulses. *Electr. Eng.* **2017**, *99*, 817–826. [[CrossRef](#)]
80. Metwally, I.A. Self-integrating Rogowski coil for high-impulse current measurement. *IEEE Trans. Instrum. Meas.* **2009**, *59*, 353–360. [[CrossRef](#)]
81. Han, R.-Y.; Wu, J.-W.; Ding, W.-D.; Jing, Y.; Zhou, H.-B.; Liu, Q.-J.; Qiu, A.-C. Hybrid PCB Rogowski coil for measurement of nanosecond-risetime pulsed current. *IEEE Trans. Plasma Sci.* **2015**, *43*, 3555–3561. [[CrossRef](#)]
82. Kumar, C.L.G.P.; Khalid, N.H.A.; Ahmad, M.H.; Nawawi, Z.; Sidik, M.A.B.; Jambak, M.I.; Kurnia, R.F.; Waldi, E.P. Development and Validation of Rogowski Coil with Commercial High Frequency Current Transformer for Partial Discharge Detection. In Proceedings of the 2018 International Conference on Electrical Engineering and Computer Science (ICECOS), Pangkal Pinang, Indonesia, 2–4 October 2018; pp. 315–320.
83. Shafiq, M.; Kutt, L.; Lehtonen, M.; Nieminen, T.; Hashmi, M. Parameters identification and modeling of high-frequency current transducer for partial discharge measurements. *IEEE Sens. J.* **2012**, *13*, 1081–1091. [[CrossRef](#)]
84. Sharifinia, S.; Allahbakhshi, M.; Ghanbari, T.; Akbari, A.; Mirzaei, H.R. A New Application of Rogowski Coil Sensor for Partial Discharge Localization in Power Transformers. *IEEE Sens. J.* **2021**, *21*, 10743–10751. [[CrossRef](#)]
85. Waldi, E.P.; Lestari, A.I.; Fernandez, R.; Mulyadi, S.; Murakami, Y.; Hozumi, N. Rogowski coil sensor in the digitization process to detect partial discharge. *Telecommun. Comput. Electron. Control.* **2020**, *18*, 1062–1071. [[CrossRef](#)]
86. Liu, X.; Huang, H.; Dai, Y. Effect of frequency on the linearity of double-layer and single-layer Rogowski coils. *IEEE Sens. J.* **2020**, *20*, 9910–9918. [[CrossRef](#)]
87. Ardila-Rey, J.A.; Barrieto, A.; Zerene, A.; de Castro, B.A.; Ulson, J.A.C.; Mas’ud, A.A.; Valdivia, P. Behavior of an inductive loop sensor in the measurement of partial discharge pulses with variations in its separation from the primary conductor. *Sensors* **2018**, *18*, 2324. [[CrossRef](#)]
88. Rojas-Moreno, M.V.; Robles, G.; Mart’ J.M.; Sanz-Feito, J. Self-integrating inductive loop for measuring high frequency pulses. *Rev. Sci. Instrum.* **2011**, *82*, 085102. [[CrossRef](#)] [[PubMed](#)]
89. Ardila-Rey, J.A.; Montaña, J.; De Castro, B.A.; Schurch, R.; Ulson, J.A.C.; Muhammad-Sukki, F.; Bani, N.A. A comparison of inductive sensors in the characterization of partial discharges and electrical noise using the chromatic technique. *Sensors* **2018**, *18*, 1021. [[CrossRef](#)]
90. Imburgia, A.; Kaziz, S.; Romano, P.; Flandre, D.; Artale, G.; Rizzo, G.; Viola, F.; Tounsi, F.; Ala, G. Investigation of PCB-based Inductive Sensors Orientation for Corona Partial Discharge Detection. In Proceedings of the 2022 IEEE 21st Mediterranean Electrotechnical Conference (MELECON), Palermo, Italy, 14–16 June 2022; pp. 559–563.
91. Lopez-Roldan, J.; Tang, T.; Gaskin, M. Optimisation of a sensor for onsite detection of partial discharges in power transformers by the UHF method. *IEEE Trans. Dielectr. Electr. Insul.* **2008**, *15*, 1634–1639. [[CrossRef](#)]
92. Jin, Z.; Sun, C.; Cheng, C.; Li, J. Two types of compact UHF antennas for partial discharge measurement. In Proceedings of the 2008 International Conference on High Voltage Engineering and Application, Chongqing, China, 19–12 November 2008; pp. 616–620.
93. Widjaja, C.D.; Fahren, A.A.M.; Khayam, U.; Hidayat, S. Design of Loop Antenna as Partial Discharge Sensor on Metal-Enclosed Power Apparatus. In Proceedings of the 2020 IEEE Region 10 Symposium (TENSYP), Dhaka, Bangladesh, 5–7 June 2020; pp. 1506–1510.
94. Ye, H.-F.; Qian, Y.; Dong, Y.; Sheng, G.H.; Jiang, X.C. Development of multi-band ultra-high-frequency sensor for partial discharge monitoring based on the meandering technique. *IET Sci. Meas. Technol.* **2014**, *8*, 327–335.
95. Zeidi, N.; Kaziz, S.; Said, M.H.; Rufer, L.; Cavallini, A.; Tounsi, F. Partial discharge detection with on-chip spiral inductor as a loop antenna. *Rev. Sci. Instrum.* **2021**, *92*, 094701. [[CrossRef](#)] [[PubMed](#)]
96. Mor, A.R.; Heredia, L.C.; Muñoz, F. A magnetic loop antenna for partial discharge measurements on GIS. *Int. J. Electr. Power Energy Syst.* **2020**, *115*, 105514.
97. Rodrigo-Mor, A.; Muñoz, F.A.; Castro-Heredia, L.C. A novel antenna for partial discharge measurements in GIS based on magnetic field detection. *Sensors* **2019**, *19*, 858. [[CrossRef](#)]
98. Hussain, G.A.; Zaher, A.A.; Hummes, D.; Safdar, M.; Lehtonen, M. Hybrid sensing of internal and surface partial discharges in air-insulated medium voltage switchgear. *Energies* **2020**, *13*, 1738. [[CrossRef](#)]

99. Chen, G.; Tao, J.; Ma, Y.; Fu, H.; Liu, Y.; Zhou, Z.; Huang, C.; Guo, C. On-site portable partial discharge detection applied to power cables using HFCT and UHF methods. *WSEAS Trans. Circuits Syst.* **2016**, *15*, 83–90.
100. Khan, A.A.; Malik, N.; Al-Arainy, A.; Alghuweinem, S. Investigation of attenuation characteristics of PD pulse during propagation in XLPE cable. In Proceedings of the 2013 IEEE Power & Energy Society General Meeting, Vancouver, BC, Canada, 21–25 July 2013; pp. 1–5.
101. Tang, J.; Zhou, Q.; Tang, M.; Xie, Y. Study on mathematical model for VHF partial discharge of typical insulated defects in GIS. *IEEE Trans. Dielectr. Electr. Insul.* **2007**, *14*, 30–38. [[CrossRef](#)]
102. Thungsook, K.; Pattanadach, N.; Nimsanong, P.; Srinangyam, C. The Bandwidth Verification of VHF Antenna and Apply for Partial Discharge Measurement. In Proceedings of the 2022 9th International Conference on Condition Monitoring and Diagnosis (CMD), Kitakyushu, Japan, 13–18 November 2022; pp. 559–562.
103. Maneerot, S.; Kando, M.; Pattanadach, N. Applying HF and VHF/UHF Partial Discharge Detection for Distribution Transformer. *J. Mob. Multimed.* **2019**, *15*, 357–376. [[CrossRef](#)]
104. Saktioto; Soerbakti, Y.; Syahputra, R.F.; Gamal, M.D.H.; Irawan, D.; Putra, E.H.; Darwis, R.S. Improvement of low-profile microstrip antenna performance by hexagonal-shaped SRR structure with DNG metamaterial characteristic as UWB application. *Alex. Eng. J.* **2022**, *61*, 4241–4252. [[CrossRef](#)]
105. Albarracin, R.; Ardila-Rey, J.A.; Masiud, A.A. On the use of monopole antennas for determining the effect of the enclosure of a power transformer tank in partial discharges electromagnetic propagation. *Sensors* **2016**, *16*, 148. [[CrossRef](#)]
106. Sikorski, W.; Szymczak, C.; Siod, K.; Polak, F. Hilbert curve fractal antenna for detection and on-line monitoring of partial discharges in power transformers. *Eksploat. Niezawodn.* **2018**, *20*, 343–351. [[CrossRef](#)]
107. Li, J.; Cheng, C.; Bao, L.; Jiang, T. Resonant frequency calculation and optimal design of peano fractal antenna for partial discharge detection. *Int. J. Antennas Propag.* **2012**, *2012*, 361517. [[CrossRef](#)]
108. Li, J.; Li, X.; Du, L.; Cao, M.; Qian, G. An intelligent sensor for the ultra-high-frequency partial discharge online monitoring of power transformers. *Energies* **2016**, *9*, 383. [[CrossRef](#)]
109. Wang, Y.; Wang, Z.; Li, J. UHF Moore fractal antennas for online GIS PD detection. *IEEE Antennas Wirel. Propag. Lett.* **2016**, *16*, 852–855. [[CrossRef](#)]
110. Li, M.; Guo, C.; Peng, Z. Design of meander antenna for UHF partial discharge detection of transformers. *Sens. Transducers* **2014**, *171*, 232.
111. Li, J.; Jiang, T.; Cheng, C.; Wang, C. Hilbert fractal antenna for UHF detection of partial discharges in transformers. *IEEE Trans. Dielectr. Electr. Insul.* **2013**, *20*, 2017–2025. [[CrossRef](#)]
112. Zahed, A.H.; Harbaji, M.M.; Habboub, S.A.; AlMajidi, M.A.; Assaf, M.J.; El-Hag, A.H.; Qaddoumi, N.N. Design of hilbert fractal antenna for partial discharge detection and classification. In Proceedings of the 2015 4th International Conference on Electric Power and Energy Conversion Systems (EPECS), Sharjah, United Arab Emirates, 24–26 November 2015; pp. 1–4.
113. Darmawan, M.A.; Khayam, U. Design, simulation, and fabrication of second, third, and forth order Hilbert antennas as ultra high frequency partial discharge sensor. In Proceedings of the Joint International Conference on Electric Vehicular Technology and Industrial, Mechanical, Electrical and Chemical Engineering (ICEVT & IMECE), Surakarta, Indonesia, 4–5 November 2015; pp. 319–322.
114. Salah, W.S.; Gad, A.H.; Attia, M.A.; Eldebeikye, S.M.; Salama, A.R. Design of a compact ultra-high frequency antenna for partial discharge detection in oil immersed power transformers. *Ain Shams Eng. J.* **2022**, *13*, 101568. [[CrossRef](#)]
115. Wang, F.; Bin, F.; Sun, Q.; Fan, J.; Liang, F.; Xiao, X. A novel uhf m inkowski fractal antenna for partial discharge detection. *Microw. Opt. Technol. Lett.* **2017**, *59*, 1812–1819. [[CrossRef](#)]
116. Ediriweera, W.; Priyanayana, K.; Rajakaruna, R.; Ranasinghe, R.; Lucas, J.; Samarasinghe, R. Microstrip Patch Antenna for Partial Discharge detection as a condition monitoring tool of power system assets. In Proceedings of the 2017 Moratuwa Engineering Research Conference (MERCOn), Moratuwa, Sri Lanka, 29–31 May 2017; pp. 368–372.
117. Sarkar, B.; Mishra, D.; Koley, C.; Roy, N. Microstrip patch antenna based UHF sensor for detection of partial discharge in high voltage electrical equipments. In Proceedings of the 2014 Annual IEEE India Conference (INDICON), Pune, India, 11–13 December 2014; pp. 1–6.
118. Xavier, G.V.; da Costa, E.G.; Serres, A.J.; Nobrega, L.A.; Oliveira, A.C.; Sousa, H.F. Design and application of a circular printed monopole antenna in partial discharge detection. *IEEE Sens. J.* **2019**, *19*, 3718–3725. [[CrossRef](#)]
119. Cruz, J.N.; Serres, A.J.R.; de Oliveira, A.C.; Xavier, G.V.R.; de Albuquerque, C.C.R.; da Costa, E.G.; Freire, R.C.S. Bio-inspired printed monopole antenna applied to partial discharge detection. *Sensors* **2019**, *19*, 628. [[CrossRef](#)] [[PubMed](#)]
120. Yang, F.; Peng, C.; Yang, Q.; Luo, H.; Ullah, I.; Yang, Y. An UWB printed antenna for partial discharge UHF detection in high voltage switchgears. *Prog. Electromagn. Res. C* **2016**, *69*, 105–114. [[CrossRef](#)]
121. Luo, H.; Cheng, P.; Liu, H.; Kang, K.; Yang, F.; Liu, K. Research on the UHF microstrip antenna for partial discharge detection in high voltage switchgear. In Proceedings of the 2016 IEEE 11th Conference on Industrial Electronics and Applications (ICIEA), Hefei, China, 5–7 June 2016; pp. 2273–2276.
122. Uwiringiyimana, J.P.; Khayam, U.; Suwarno; Montanari, G.C. Design and Implementation of Ultra-Wide Band Antenna for Partial Discharge Detection in High Voltage Power Equipment. *IEEE Access* **2022**, *10*, 10983–10994. [[CrossRef](#)]



123. Lozano-Claros, D.; Custovic, E.; Elton, D. Two planar antennas for detection of partial discharge in gas-insulated switchgear (GIS). In Proceedings of the 2015 IEEE International Conference on Communication, Networks and Satellite (COMNESTAT), Bandung, Indonesia, 10–12 December 2015; pp. 8–15.
124. Park, S.; Jung, K.-Y. Design of a circularly-polarized UHF antenna for partial discharge detection. *IEEE Access* **2020**, *8*, 81644–81650. [[CrossRef](#)]
125. Yadam, Y.R.; Sarathi, R.; Arunachalam, K. Planar Ultrawideband Circularly Polarized Cosine Slot Archimedean Spiral Antenna for Partial Discharge Detection. *IEEE Access* **2022**, *10*, 35701–35711. [[CrossRef](#)]
126. Li, T.; Rong, M.; Zheng, C.; Wang, X. Development simulation and experiment study on UHF partial discharge sensor in GIS. *IEEE Trans. Dielectr. Electr. Insul.* **2012**, *19*, 1421–1430. [[CrossRef](#)]
127. Cheng, L.; Wen, H.; Liu, Y.; Jiang, Y.; Zhou, Z.; Zhang, J.; Zhang, G.; Mao, H. Study on Flexible Built-in Miniature Archimedes Spiral Antenna Sensor for High-voltage electrical equipment PD Detection. In Proceedings of the 2022 7th Asia Conference on Power and Electrical Engineering (ACPEE), Hangzhou, China, 15–17 April 2022; pp. 1477–1482.
128. Andre, H.; Emeraldi, P.; Hazmi, A.; Waldi, E.P.; Khayam, U. Long bowtie antenna for partial discharge sensor in gas-insulated substation. In Proceedings of the 2017 International Conference on High Voltage Engineering and Power Systems (ICHVEPS), Bali, Indonesia, 2–5 October 2017; pp. 175–178.
129. Rhamdhani, T.; Khayam, U.; Zaeni, A. Improving Antenna Performance by Combining Dipole and Bowtie Antenna for Partial Discharge Measurement in Gas Insulated Switchgear. In Proceedings of the 2022 IEEE International Conference in Power Engineering Application (ICPEA), Shah Alam, Malaysia, 7–8 March 2022; pp. 1–4.
130. Daulay, M.S.H.; Khayam, U. New Design of Double Layer Bow-tie Antenna with Edge and Middle Sliced Modification for Partial Discharge Measurement. In Proceedings of the 2018 Conference on Power Engineering and Renewable Energy (ICPERE), Surakarta, Indonesia, 29–31 October 2018; pp. 1–5.
131. Uwiringiyimana, J.P.; Khayam, U. Measurement of partial discharge in air insulation by using UHF double layer bowtie antenna with modified wings edges. In Proceedings of the 2019 International Conference on Electrical Engineering and Informatics (ICEEI), Bandung, Indonesia, 9–10 July 2019; pp. 228–233.
132. Zhang, J.; Zhang, X.; Xiao, S. Antipodal Vivaldi antenna to detect uhf signals that leaked out of the joint of a transformer. *Int. J. Antennas Propag.* **2017**, *2017*, 9627649. [[CrossRef](#)]
133. Saleh, S.; Ismail, W.; Abidin, I.S.Z.; Bataineh, M.H.; Alzoubi, A.S. Compact UWB Vivaldi Tapered Slot Antenna. *Alex. Eng. J.* **2022**, *61*, 4977–4994. [[CrossRef](#)]
134. Albarracin, R.; Robles, G.; Mart', J.; Ardila-Rey, J. Separation of sources in radiofrequency measurements of partial discharges using time-power ratio maps. *ISA Trans.* **2015**, *58*, 389–397. [[CrossRef](#)] [[PubMed](#)]
135. Harbaji, M.M.; Zahed, A.H.; Habboub, S.A.; AlMajidi, M.A.; Assaf, M.J.; El-Hag, A.H.; Qaddoumi, N.N. Design of Hilbert fractal antenna for partial discharge classification in oil-paper insulated system. *IEEE Sens. J.* **2016**, *17*, 1037–1045. [[CrossRef](#)]
136. Uwiringiyimana, J.P.; Suwarno; Khayam, U. Design of an Ultra-Wide Band Microstrip Patch Antenna for Partial Discharge Detection on Power Transformer. In Proceedings of the 2021 IEEE International Conference on the Properties and Applications of Dielectric Materials (ICPADM), Johor Bahru, Malaysia, 11–15 July 2021; pp. 242–245.
137. Sinaga, H.H. Detection, Identification and Localization of Partial Discharges in Power Transformers Using UHF Techniques. Ph.D. Thesis, The University of New South Wales Australia, Sydney, Australia, 2012.
138. Chai, H.; Phung, B.; Zhang, D. Development of UHF sensors for partial discharge detection in power transformer. In Proceedings of the 2018 Condition Monitoring and Diagnosis (CMD), Perth, Australia, 23–26 September 2018; pp. 1–5.
139. Zhang, X.; Cheng, Z.; Gui, Y. Design of a new built-in UHF multi-frequency antenna sensor for partial discharge detection in high-voltage switchgears. *Sensors* **2016**, *16*, 1170. [[CrossRef](#)]
140. Khosronejad, M.; Gentili, G.G. Design of an Archimedean spiral UHF antenna for pulse monitoring application. In Proceedings of the 2015 Loughborough Antennas Propagation Conference (LAPC), Leicestershire, UK, 2–3 November 2015; pp. 1–4.

**Disclaimer/Publisher's Note:** The statements, opinions and data contained in all publications are solely those of the individual author(s) and contributor(s) and not of MDPI and/or the editor(s). MDPI and/or the editor(s) disclaim responsibility for any injury to people or property resulting from any ideas, methods, instructions or products referred to in the content.